AIMS Mathematics, 7(11): 20341–20369.
DOI: 10.3934/math.20221114
Received: 02 June 2022
Revised: 06 August 2022
Accepted: 16 August 2022
Published: 16 September 2022

http://www.aimspress.com/journal/Math

Research article

Intelligent computing based supervised learning for solving nonlinear system of malaria endemic model

Iftikhar Ahmad[1], Hira Ilyas[1], Muhammad Asif Zahoor Raja[2,*], Tahir Nawaz Cheema[1], Hasnain Sajid[1], Kottakkaran Sooppy Nisar[3,*], Muhammad Shoaib[4], Mohammed S. Alqahtani[5,6], C Ahamed Saleel[7] and Mohamed Abbas[8,9]

[1] Department of Mathematics, University of Gujrat, Gujrat, 50700, Pakistan

[2] Future Technology Research Center, National Yunlin University of Science and Technology, 123 University Road, Section 3, Douliou, Yunlin 64002, Taiwan, China

[3] Department of Mathematics, College of Arts and Sciences, Wadi Aldawaser, 11991, Prince Sattam bin Abdulaziz University, Saudi Arabia

[4] Department of Mathematics, COMSATS University Islamabad, Attock Campus, Pakistan

[5] Radiological Sciences Department, College of Applied Medical Sciences, King Khalid University, Abha 61421, Saudi Arabia

[6] BioImaging Unit, Space Research Centre, Michael Atiyah Building, University of Leicester, Leicester, LE1 7RH, U.K

[7] Department of Mechanical Engineering, College of Engineering, King Khalid University, Asir-Abha, 61421, Saudi Arabia

[8] Electrical Engineering Department, College of Engineering, King Khalid University, Abha 61421, Saudi Arabia

[9] Electronics and communications Department, College of Engineering, Delta University for Science and Technology, Gamasa 35712, Egypt

* **Correspondence:** Email: n.sooppy@psau.edu.sa, rajamaz@yuntech.edu.tw.

Abstract: A repeatedly infected person is one of the most important barriers to malaria disease eradication in the population. In this article, the effects of recurring malaria re-infection and decline in the spread dynamics of the disease are investigated through a supervised learning based neural networks model for the system of non-linear ordinary differential equations that explains the mathematical form of the malaria disease model which representing malaria disease spread, is divided into two types of systems: Autonomous and non-autonomous, furthermore, it involves the parameters of interest in terms of Susceptible people, Infectious people, Pseudo recovered people, recovered people prone to re-infection, Susceptible mosquito, Infectious mosquito. The purpose of this work

is to discuss the dynamics of malaria spread where the problem is solved with the help of Levenberg-Marquardt artificial neural networks (LMANNs). Moreover, the malaria model reference datasets are created by using the strength of the Adams numerical method to utilize the capability and worth of the solver LMANNs for better prediction and analysis. The generated datasets are arbitrarily used in the Levenberg-Marquardt back-propagation for the testing, training, and validation process for the numerical treatment of the malaria model to update each cycle. On the basis of an evaluation of the accuracy achieved in terms of regression analysis, error histograms, mean square error based merit functions, where the reliable performance, convergence and efficacy of design LMANNs is endorsed through fitness plot, auto-correlation and training state.

Keywords: neural networks; Levenberg-Marquardt artificial neural networks; supervised learning
Mathematics Subject Classification: 68T07, 92B20

1. Introduction

Malaria is a mosquito-borne disease that is spread by one-celled Plasmodium parasites [1]. Malaria's ability to continue increasing mortality and morbidity causes significant public health and economic challenges in developing countries [2]. About two billion people are constantly at risk of infection around the world [3], some areas of Africa have been severely affected, with children and women making up the majority of the victims. Malaria kills at least one millions of people per year in Sub-Saharan Africa, according to the World Health Organization (WHO) and it has the potential to become even worse as a result of climate change and the (HIV) [4,5]. Malaria spread in humans by bites from an infected anopheles Mosquito. Medical symptoms including discomfort, headaches, body aches, fever, nausea, sweats and vomiting appear a few days after the bites. After a blood meal, mosquitoes collect infection from an infected person. Malaria is a life-threatening disease that can be prevented and treated if caught early. Current methods of controlling the disease include pesticides, medicines, treated bed nets and treatments to prevent the disease. In certain areas, these measures resulted in significant reductions in morbidity and mortality [6]. However, if the disease is not managed appropriately and treated, symptoms may worsen. The most significant impediment to malaria elimination is the occurrence of recurring malaria, which can be categorized as relapse and re-infection [7,8]. On the other hand, the appearance of the relapse symptoms of recurrence of non-parasites in the liver, such as later the parasites have cleared their blood [9–11]. Reinfection, on the other hand, is not caused by medication failure; rather, it is the recurrence of malaria diseases reported by parasite infection from innovative infectious mosquito bites.

Various mathematical models (see, for example, [12–15]), which describe the dynamic transmission of malaria population has evolved since the early works of May and Anderson [16], Macdonald [17], and Ross [18]. Anguelov et al. [12] suggested a mathematical model that would use sterile insect technology to reduce the number of wild lady anospheles mosquitos. Ghosh [13] has developed a model of the dynamics of malaria with this assumption after the density of the mosquito population increased in terms of the attractiveness of the environment. The authors of [14] used the stability principle of differential equations to investigate malaria dynamic behavior with nonlinear infection forces. Niger and Gumel [19] developed a deterministic model to evaluate the impact of re-infection

on the dynamics of malaria transmission. The impact of relapse on the slow and fast dynamics of a malaria disease model were studied by Li et al. [20]. The authors of [21] investigated a malaria model in which the recovered people not only arrival to the susceptible individuals class, but also back to the infectious individuals class (relapse). A number of many other mathematical malaria models of relapse have been discussed in the works [22–24]. However, we have implemented a complex model of six classes based on the current scenarios, Susceptible people (S_1), infectious people (I_1), pseudo recovered people (R_1), Recovered people prone to re-infection (R_2), mosquito Susceptible (S_2) and mosquito infection (I_2) classes, i.e. malaria model for numerical investigation [25]. Recently, the proposed malaria model is mathematically analysis through various methods some of them as [26–29].

The power of artificial intelligence-based computing solvers has been misused, leading to the widespread application of technology and applied science to estimate and solve many problems. Recent research in bioinformatics, reactive transport systems, nano-fluidics, atomic physics, plasma physics, electricity energy, nanotechnology, Van-der-Pol oscillatory systems, entropy optimization system in the fluid flow system and functional mathematics has been reported to be of paramount importance (see [30–43] and references cited in it). The above outcomes are motivational affinities for the malaria model to investigate in the artificial intelligence base, numerical computing solver. According to our review of the literature, Levenberg-Marquardt artificial neural networks (LMANNs) have yet to be used to resolve initial value problems (IVBs) of non-linear ordinary differential equation (ODE) systems that describe malaria dynamics. The following is an emphasis on the revolutionary contributions of the work to be implemented in malaria models for Levenberg-Marquardt artificial neural networks (LMANNs).

- The effect of the malaria model, which is expressed by a non-linear system containing six ordinary differential equations corresponding to the initial value problems (IVPs), is investigated using the supervised learning infrastructure based on 2 layers structure of the Levenberg-Marquardt artificial neural networks (LMANNs).
- Using the Adams numerical method, the mean square error (MSE) analysis of computationally achieved results to compute merit function designed by LMANNs considering six class reference solutions based on malaria epidemic model performed efficiently by index. Moreover, the comparative study validates the outcomes attained through the designed solver.
- Levenberg-Marquardt back-propagation is used to carry through validation, testing, and training in order to obtain decision variables for artificial neural networks (ANNs) for each epoch index increment. To meet this goal, we have considered a model of six complex classes based on the Susceptible people (S_1), the infections people (I_1), the Pseudo recovered people (R_1), the recovered people prone to re-infection (R_2), the susceptible mosquitoes (S_2) and the infections mosquitoes (I_2).
- Accurate performance, convergence and reliability of (LMANNs) to resolve the malaria model with reference dataset for variation of two different parameters are endorsed by correlation, regression curve and histograms with error analysis and comparative study.

Section 2 provides a brief description of mathematical models of the malaria consisting system of nonlinear differential equations, LMANNs methodology is given in Sect. 3, the numerical analysis and discussion are provided in Sect. 4 for various cases of malaria dynamics, we conclude the research article in the last section.

2. Modelling of mathematical for malaria models

The following 4 classes of the human population are considered for the development of transmission dynamics with the rehabilitation and re-infection of the malaria model, namely, the $S_1(t)$ denoted susceptible people class at time t, $I_1(t)$ is an infectious people class, $R_1(t)$ denotes a pseudo-recovered people with the possibility of infection reactivation (relapse), and $R_2(t)$ is a recovered people with the possibility of re-infection. Hence, the total number of human population $N_1(t)$ is calculated as follows: $N_1(t) = S_1(t) + I_1(t) + R_1(t) + R_2(t)$, on the other hand, the total number of mosquito population $N_2(t)$ is divided into 2 groups: susceptible class $S_2(t)$ and infectious class $I_2(t)$, $N_2(t) = S_2(t) + I_2(t)$ The dynamics of malaria transmission, including re-infection and relapse, are defined by the system of non-linear initial value problem for deterministic mathematical model below;

$$\frac{dS_1}{dt} = \lambda_1 - \frac{\phi_1 \alpha S_1(t) V_1(t)}{N_1} - \delta_1 S_1(t), \tag{2.1}$$

$$\frac{dI_1}{dt} = \frac{\phi_1 \alpha I_2(t)(S_1(t) + \tau R_2(t))}{N_1} - (\psi + \delta_1) I_1(t) + \eta R_1(t), \tag{2.2}$$

$$\frac{dR_1}{dt} = \rho \psi I_1(t) - (\eta + \delta_1) I_1(t), \tag{2.3}$$

$$\frac{dR_2}{dt} = (1 - \rho)\psi I_1(t) - \frac{\phi_1 \alpha \tau R_2(t) I_2(t)}{N_1} - \delta_1 R_2(t), \tag{2.4}$$

$$\frac{dS_2}{dt} = \lambda_2 - \frac{\phi_2 \alpha S_2(t)(I_2 + \beta R_1(t)}{N_1} - \delta_2 S_2, \tag{2.5}$$

$$\frac{dI_2}{dt} = \frac{\phi_2 \alpha S_2(t)(I_2 + \beta R_1(t))}{N_1} - \delta_2 I_2, \tag{2.6}$$

$$S_1[0] = 440,\ I_1[0] = 30,\ R_1[0] = 10,\ R_2[0] = 20,\ S_2[0] = 950,\ I_2[0] = 50. \tag{2.7}$$

Where, in the nomenclature table, definitions of each parameter on the malaria model (2.1)–(2.7) are given. For the dynamics of malaria, a graphical representation of the malaria model is shown in Figure 1 to more evidently decode the information.

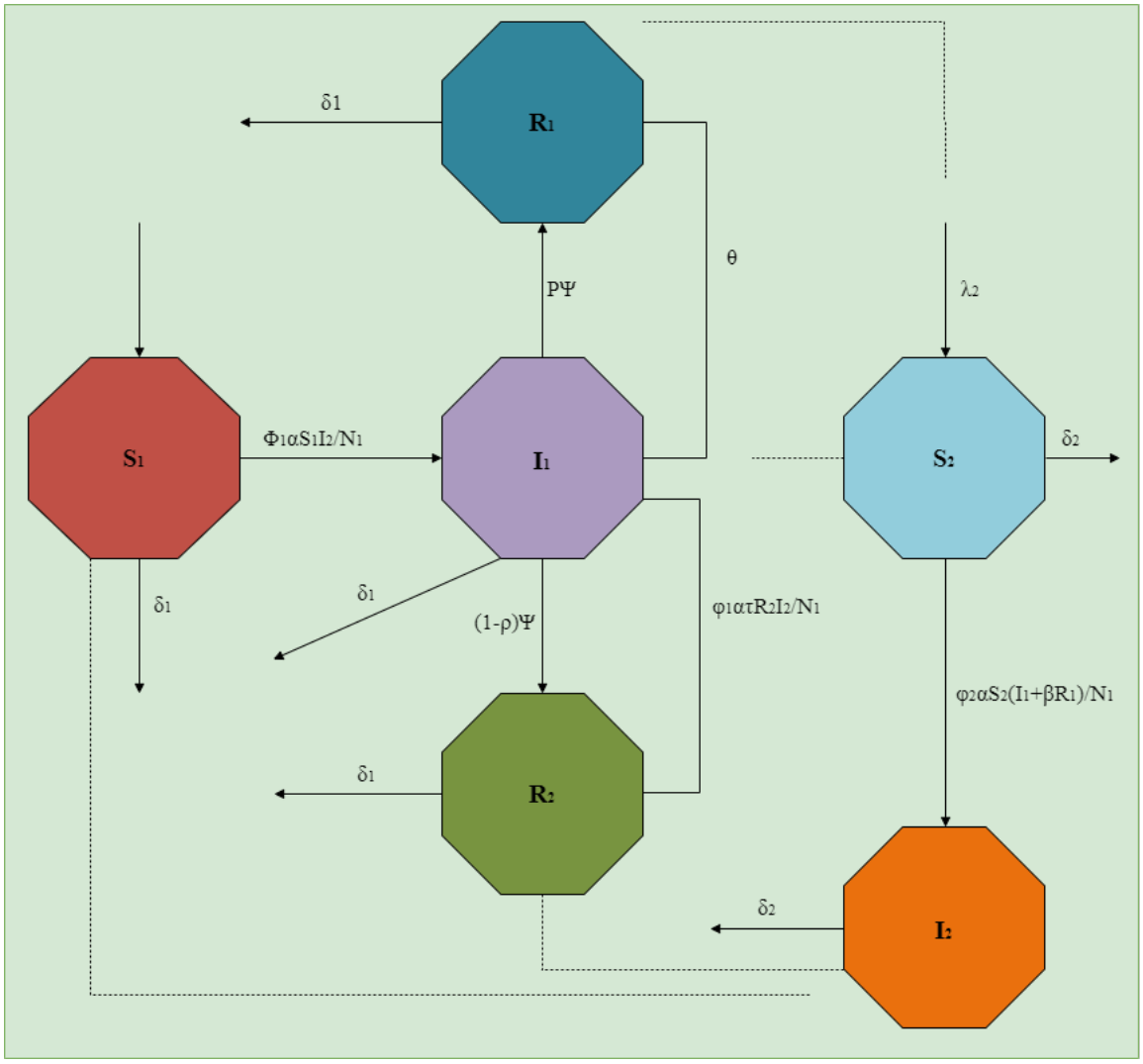

Figure 1. Six classes based deterministic mathematical model of malaria dynamics.

Consider the malaria model equations as a dynamical system

The Eqs (2.8)–(2.14) mathematical explanation of the dynamical system of the malaria model.

$$\frac{dS_1}{dt} = 100 - 1.66 \times 10^{-03} S_1(t) v_1(t) - 5.48 \times 10^{-05} S_1(t), \tag{2.8}$$

$$\frac{dI_1}{dt} = 1.66 \times 10^{-03} I_2(t)(S_1(t) + 0.85 R_2(t)) - 5.48 \times 10^{-07} I_1(t) + 2.8 \times 10^{-03} R_1(t), \tag{2.9}$$

$$\frac{dR_1}{dt} = 0.0025 I_1(t) - 2.8 \times 10^{-03} I_1(t), \tag{2.10}$$

$$\frac{dR_2}{dt} = 0.0075 I_1(t) - 1.42 \times 10^{-03} R_2(t) I_2(t) - 5.48 \times 10^{-05} R_2(t), \tag{2.11}$$

$$\frac{dS_2}{dt} = 1000 - 9.6 \times 10^{-04} S_2(t)(I_2 + 0.01 R_1(t)) - 0.066 S_2, \tag{2.12}$$

$$\frac{dI_2}{dt} = 9.6 \times 10^{-04} S_2(t)(I_2 + 0.001R_1(t)) - 0.066I_2, \tag{2.13}$$

$$S_1[0] = 440,\ I_1[0] = 30,\ R_1[0] = 10,\ R_2[0] = 20,\ S_2[0] = 950,\ I_2[0] = 50. \tag{2.14}$$

3. Methodology

This section covers the most important aspects of our proposed mathematical modelling of performance matrix. Three steps have been used to execute the mathematical modelling: In step one, the malaria model is evaluated by changing two different parameters, which is pointed to as the input reference dataset point for FFNN, step two, LMBNNs model layer structure formulation and training of LMBNNs models is considered. LMBNNs is executed in step three with Levenberg-Marquardt Solver. A graphical summary of the study presented is shown in Figure 2. It presents the Adams Predictive Accuracy Method of the system (2.8)–(2.14). To increase the level of accuracy of the results with the information provided by the predicted results, we first used the predictive solution and then the whole numerical approach using the Adams method configuration. The predictor-corrector method (2.8)–(2.14) of the equations may be given as (3.1)–(3.7).

$$\frac{dS_1}{dt} = f(t, S_1, I_1),\ S_1(t_0) = S_{1_0}, \tag{3.1}$$

$$\frac{dI_1}{dt} = f(t, S_1, I_1, R_1, R_2, V_2),\ I_1(t_0) = I_{1_0}, \tag{3.2}$$

$$\frac{dR_1}{dt} = f(t, I_1, R_1),\ R_1(t_0) = R_{1_0}, \tag{3.3}$$

$$\frac{dR_2}{dt} = f(t, I_1, R_2, I_2),\ S_1(t_0) = S_{1_0}, \tag{3.4}$$

$$\frac{dS_2}{dt} = f(t, R_1, S_2, I_2),\ S_2(t_0) = S_{2_0}, \tag{3.5}$$

$$\frac{dV_2}{dt} = f(t, R_1, S_2, I_2),\ V_2(t_0) = V_{2_0}. \tag{3.6}$$

In the case of the first equation of set (3.2)–(3.6), the relation of the predictor 2-step formula is given:

$$S_{1_{p+1}} = S_{1_p} + \frac{3}{2}hf(t_p, S_{1_p}) - \frac{1}{2}hf(t_{p-1}, S_{1_{p-1}}), \tag{3.7}$$

While, in the case of the first equation of set (3.2)–(3.6) the 2-step formula of the corrector relationship is written as:

$$S_{1_{p+1}} = S_{1_p} + \frac{1}{2}hf(t_{p+1}, S_{1_{p+1}}) + f(t_p, S_{1_p}), \tag{3.8}$$

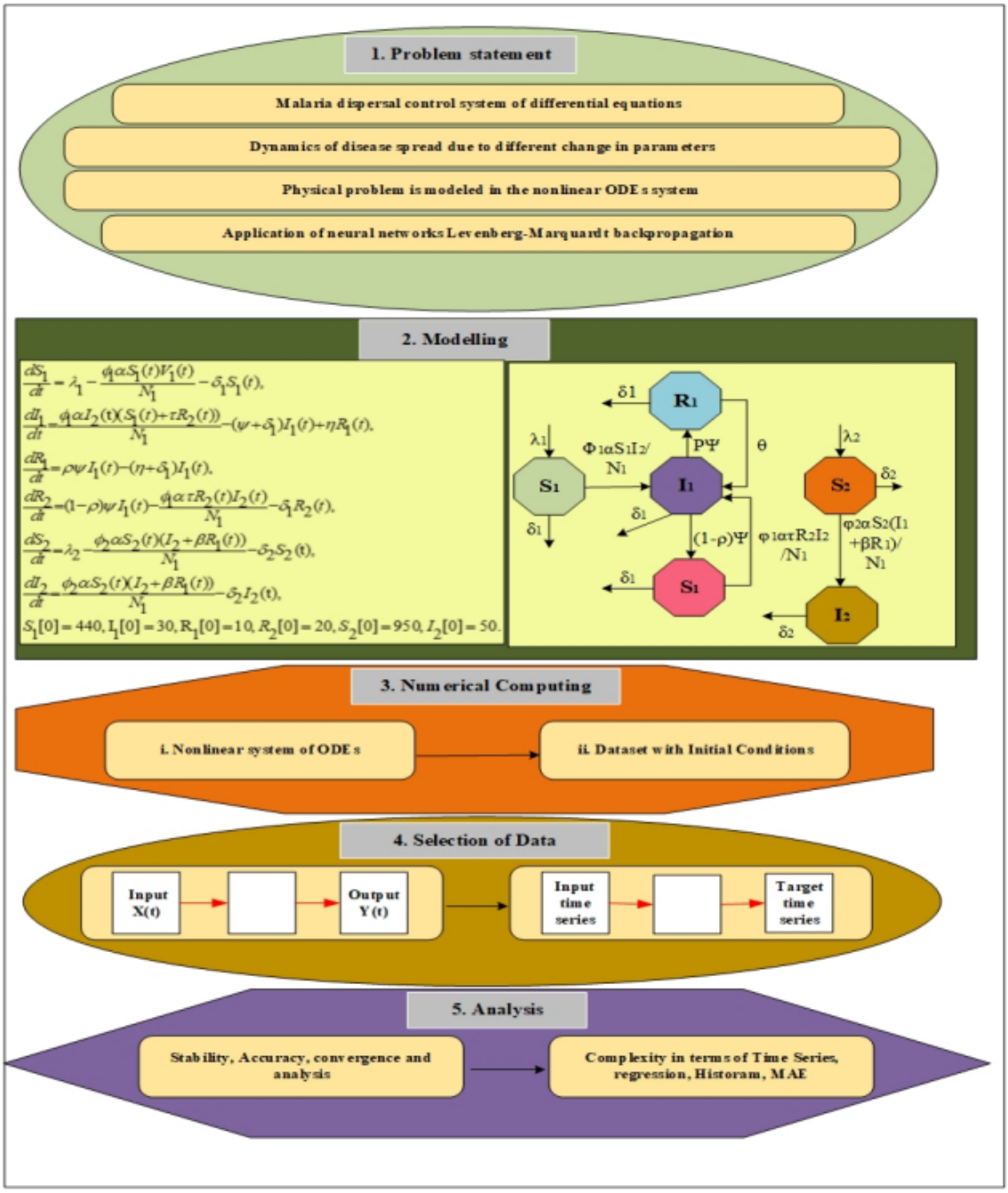

Figure 2. Procedure for the flow design of the LMANNs Projected Methodology for malaria model solving.

Accordingly, in set (3.2)–(3.6) the formulas are formulated for the predictive and accuracy method for the remaining equations. The FFNN data-set can be configured with the Adams numerical method summarized in Eqs (2.8)–(2.14) to solve the malaria model. However, in the study presented, we have developed an FFNN data-set using the mathematical NDSolve routine with the algorithm Adams' for each scenario of malaria model. To solve each scenario of the malaria model, the layer structure of

FFNN models with log sigmoid activation function and 40 numbers of neurons in the hidden layer are used. The architecture designed by FFNN is shown in Figure 3. The Levenberg-Marquardt Method (LMM) back-propagation is used to train FFNN, which entails explaining the merit function of the error basis for FFNN-LMM. The merit function of mean square error (MSE) is built on metrics and objective optimization the function is executed with LMM for each case.

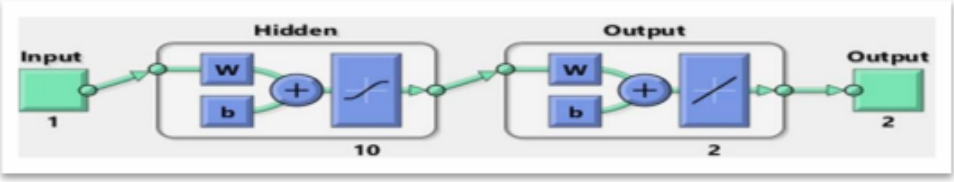

Figure 3. Function fitting neural networks.

The following is a measure of the performance of a mathematical note by AE, merit figure, i.e. MSE and regression coefficient:

$$AE = |S_q - \hat{S}_q|, \quad q = 1, 2, 3, 4, \cdots, m, \tag{3.9}$$

$$MSE = \frac{1}{m}\sum_{q=1}^{m}(S_q - \hat{S}_q)^2, \tag{3.10}$$

$$R^2 = 1 - \frac{\sum_{q=1}^{m}(S_q - \hat{S}_q)^2}{\sum_{q=1}^{m}(S_q - \overline{S}_q)^2}. \tag{3.11}$$

Here, S_q, $\hat{S}_q$ and $\overline{S}_q$ stand for reference, *qth* estimates the input solution and the means, while the m represents the total number of grids in the input. The R unit value, i.e., the parameter required for successful modeling is the square root of R^2, and the absolute and mean square error must be equal to zero for successful modeling scenarios.

4. Numerical results and discussion

Simulated studies of numbers with the necessary explanations are presented here for the first order non-linear ODE (2.1)–(2.7) system in which the malaria model by using the proposed LMANNs method. The epidemic model is represented. The values of the several parameters of the malaria model are discussed in Table 1.

Table 1. An analysis of the malaria models constant parameters and their numerical values [44].

Parameter	Description	Value
λ_1	Recruitment rate in human population	100
λ_2	Recruitment rate in mosquito population	1000
δ_1	Human mortality rate in the natural environment	5.48×10^{-05}
δ_2	Mosquito mortality rate in the natural environment	6.6×10^{-02}
β	Human infectiousness in the R_1 class caused a parameter modification	0.01
ϕ_1	Probability of infection transmission in human	0.833
ϕ_2	Probability of infection transmission in mosquitos	0.48
α	Biting rate of mosquitoes	1
η	Humans in the R1 class have a high rate of relapse	2.8×10^{-03}
τ	Human re-infection in the R_2 class caused a parameter modification	0.85
ψ	Infectious human recovery rate	0.01
ρ	Percentage of infected people who recovered	0.25

Figure 2 explain the complete process workflow diagram of the offered LMANNs. In the neural network toolbox in the Matlab setting, the offered LMANNs are implemented via 'ntstool' (neural time series tool), while Levenberg-Marquardt back-propagation is used to train neural network weights. The reference data-set of malaria model is created for 100 days as step-size inputs of 1.0 through the Adams numerical approach solutions by using the built-in Mathematica environment NDSolve function for a numerical non-linear system of ordinary differential equations results for every case of the malaria model. The values for S_1, I_1, R_1, R_2, S_2 and I_2 classes for 101 input data-set points that are randomly dispersed to yield a set for validation, testing, and training with 5%, 5%, and 90% respectively. Two layered structure LMANNs the computational model based on neural networks with Levenberg-Marquardt back production with 40 hidden layers is contracted for the results of the malaria model that shown in Figure 3.

In scenario 1 we discussed 3 different cases of changing the values of $\tau = 0.06$, 0.30 and 0.85 by keeping all other parameter are fixed to examine the behavior of Susceptible people class (S_1), infectious people class (I_1), pseudo recovered people class (R_1), Recovered people prone to re-infection class (R_2), mosquito Susceptible class (S_2) and mosquito infection class (I_2). The effects of changing the human re-infection parameter (t) and constant rate of relapse (η) on the dynamical behavior of recovered human and infectious population are shown in sub-Figure 4a-f and 5a-f. As shown in Figure 4b and 4d, increasing the re-infection parameter (τ) increases the population of infection people I_1, which reduces the human recovered population R2 over time. Similar, in scenario 2 with three different cases by changing the values of $\eta = 2.8 \times 10^{-03}$, 2.8×10^{-02} and 2.8×10^{-01} with other parameter are constant to examine the behavior of the Susceptible people class (S_1), infectious people class (I_1), pseudo recovered people class (R_1), Recovered people prone to re-infection class (R_2), mosquito Susceptible class (S_2) and mosquito infection class (I_2). It is seen in Figure 5c, increasing the constant rate of relapse (η) decrease the population pseudo recovered people.

Figures 4–15 describe comparative outcomes by graphical results of various scenarios and cases. Therefore, for the Susceptible people class (S_1), infectious people class (I_1), pseudo recovered people class (R_1), Recovered people prone to re-infection class (R_2), mosquito Susceptible class (S_2) and

mosquito infection class (I_2) the graphical and numerical outcomes of LMANNs are defined to explain the performance corresponding to 100 days for case 1 – 3 with both scenarios.

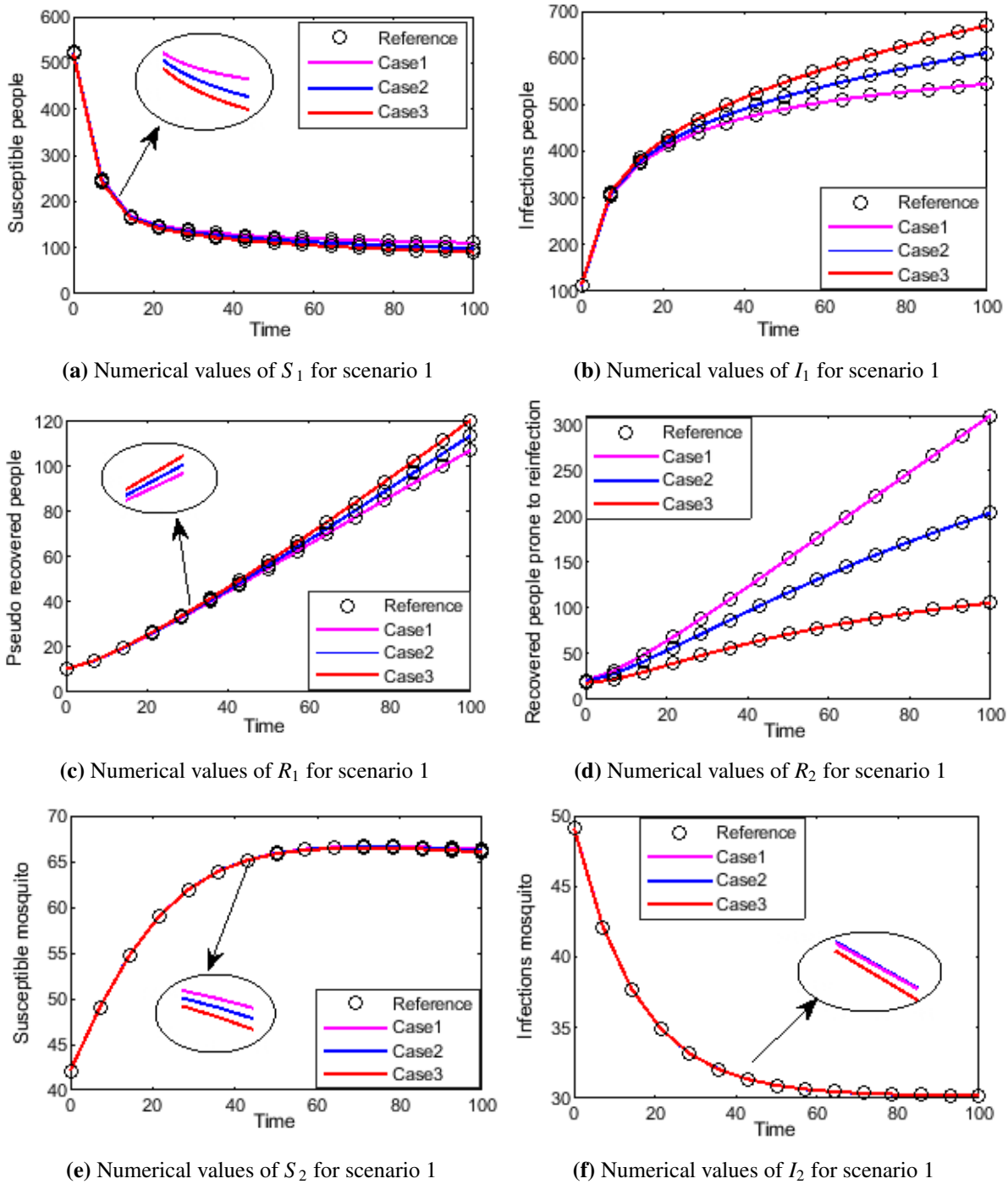

(a) Numerical values of S_1 for scenario 1

(b) Numerical values of I_1 for scenario 1

(c) Numerical values of R_1 for scenario 1

(d) Numerical values of R_2 for scenario 1

(e) Numerical values of S_2 for scenario 1

(f) Numerical values of I_2 for scenario 1

Figure 4. Analysis through suggested LMANNs with the reference numerical outcome for each classes of malaria model for scenario 1 with case 1–3.

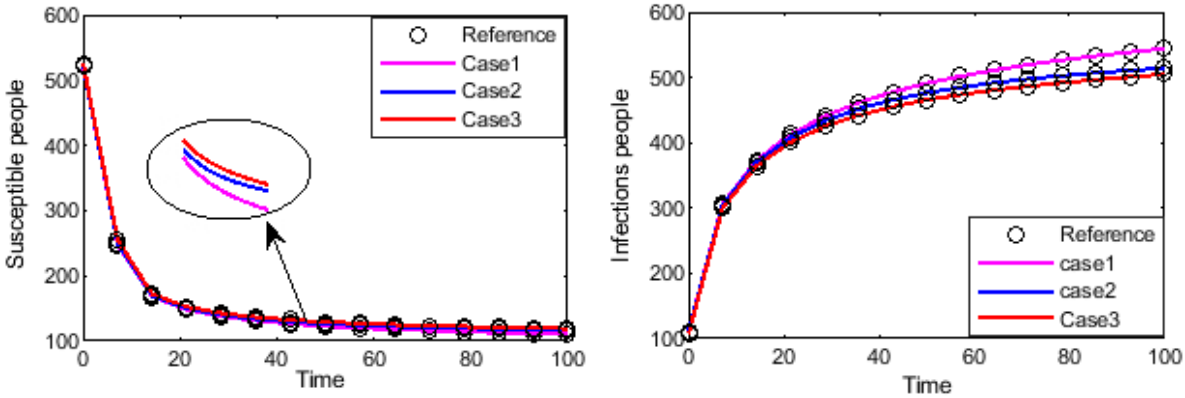

(a) Numerical values of S_1 for scenario 2

(b) Numerical values of I_1 for scenario 2

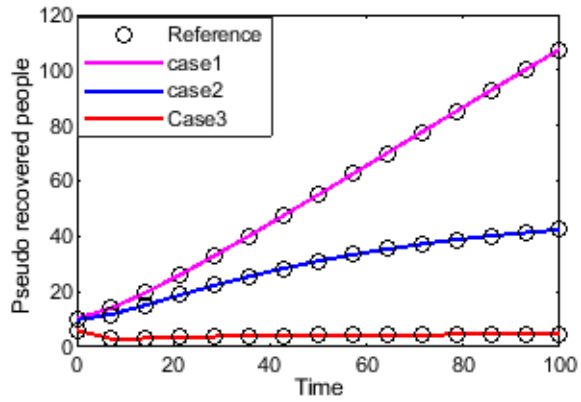

(c) Numerical values of R_1 for scenario 2

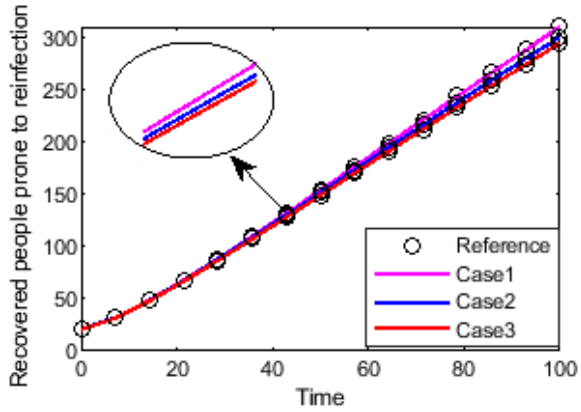

(d) Numerical values of R_2 for scenario 2

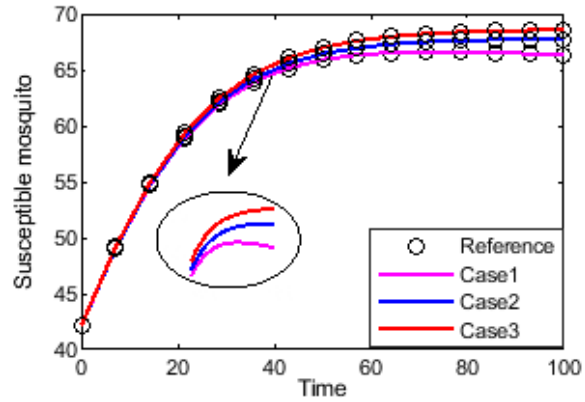

(e) Numerical values of S_2 for scenario 2

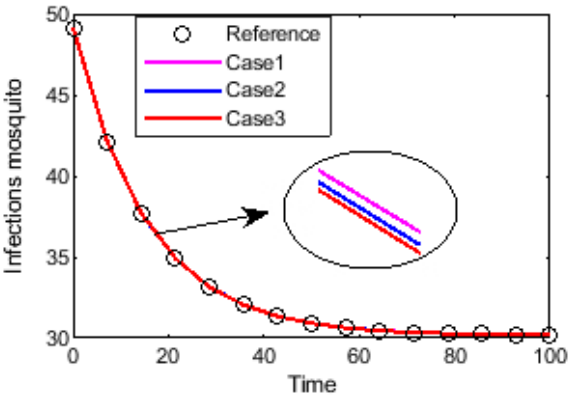

(f) Numerical values of I_2 for scenario 2

Figure 5. Analysis through suggested LMANNs with the reference numerical outcome for each classes of malaria model for scenario 2 with case 1–3.

Numerical results are represented in sub-Figure 4a-f and 5a-f. For all cases of each malaria model class, the numerical outcomes obtained by the offered technique are presented in Tables 3–8. The graphical compression is expressed by performance analysis of computational scenarios in the sub-Figure 6a, 6c, 6e, 7a, 7c and 7e. Performance consist of on mean square error (MSE) which is the

difference between simulation and observation, the less value of MSE indicates the best performance.

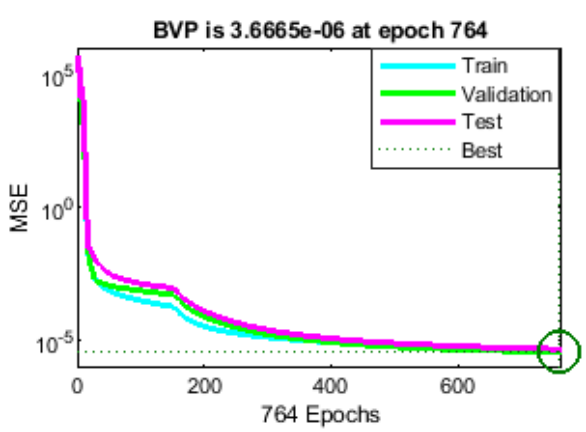

(a) Result of MSE for scenario 1 with case 1

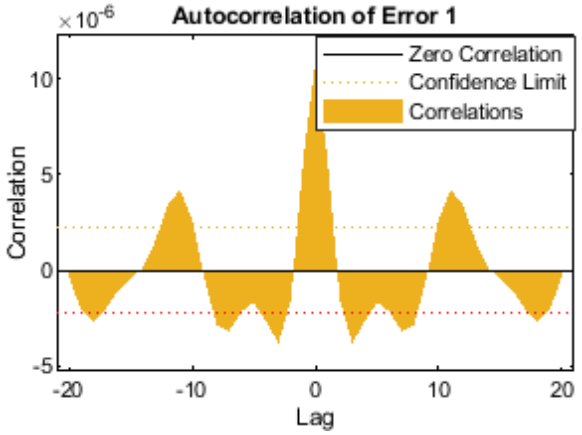

(b) Result of autocorrelation for scenario 1 with case 1

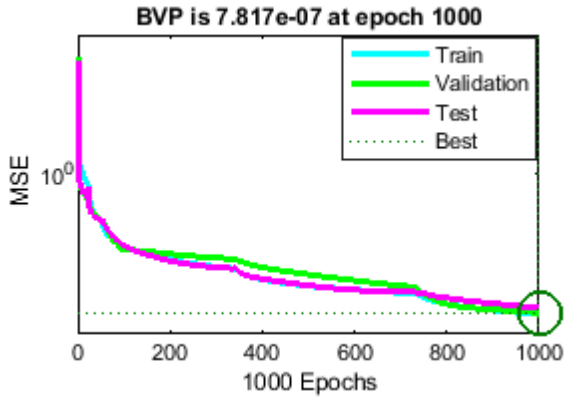

(c) Result of MSE for scenario 1 with case 2

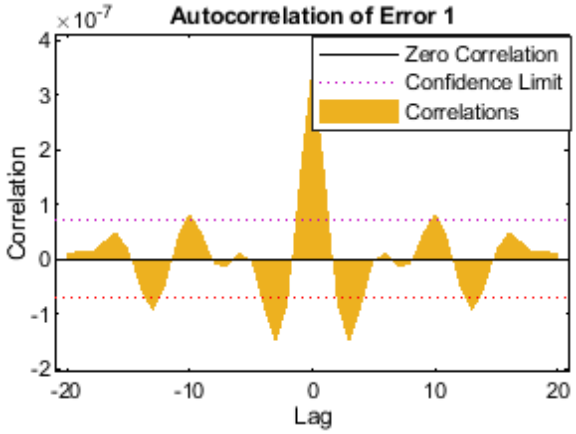

(d) Result of autocorrelation for scenario 1 with case 2

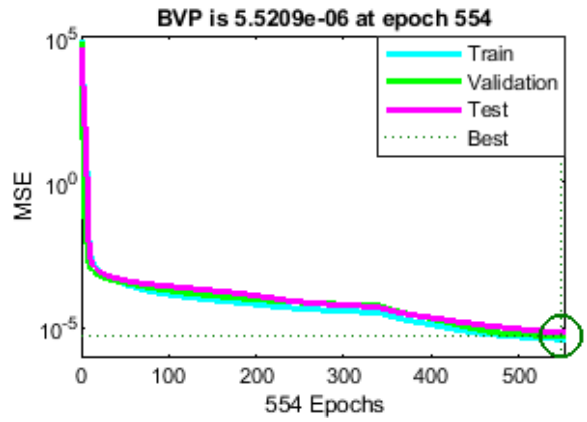

(e) Result of MSE for scenario 1 with case 3

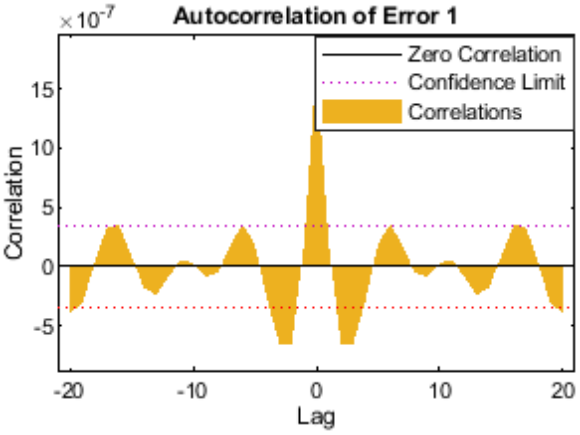

(f) Result of autocorrelation for scenario 1 with case 3

Figure 6. Comparison of mean square error (MSE) and auto-correlation for the various parameter value of case 1–3 based on malaria model with scenario 1.

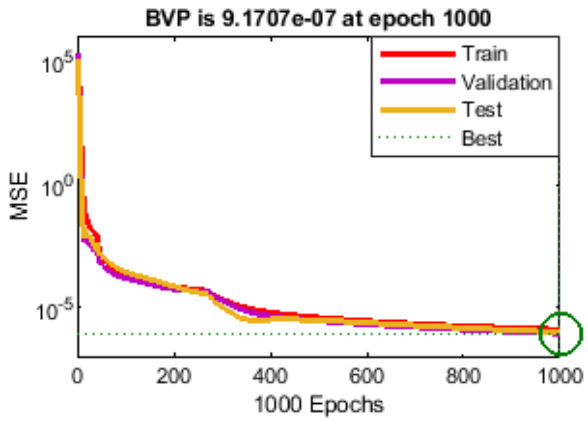

(a) Result of MSE for scenario 2 with case 1

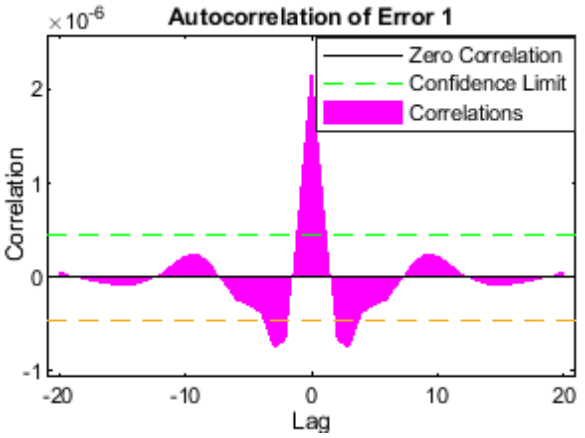

(b) Result of autocorrelation for scenario 2 with case 1

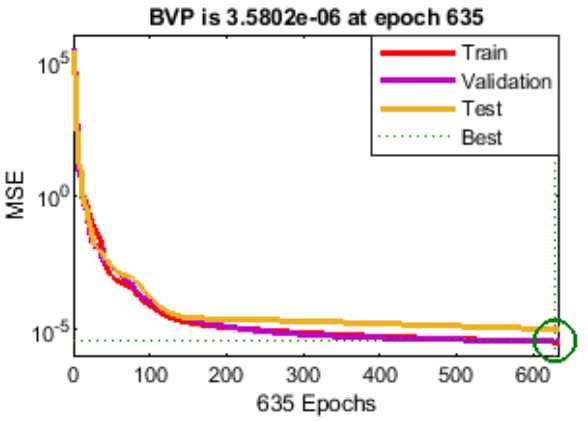

(c) Result of MSE for scenario 2 with case 2

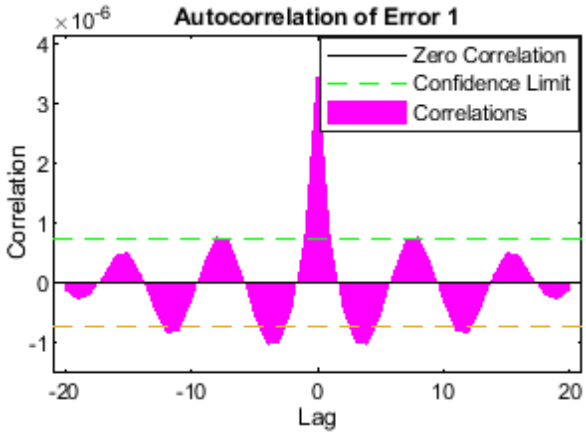

(d) Result of autocorrelation for scenario 2 with case 2

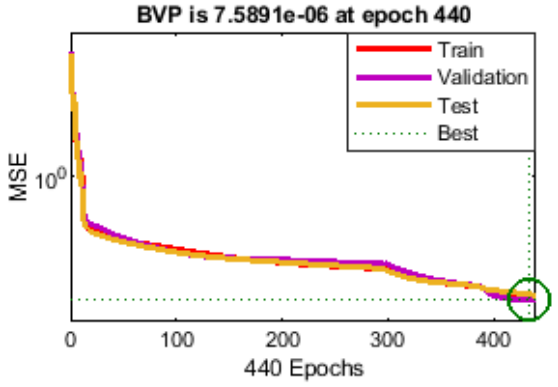

(e) Result of MSE for scenario 2 with case 3

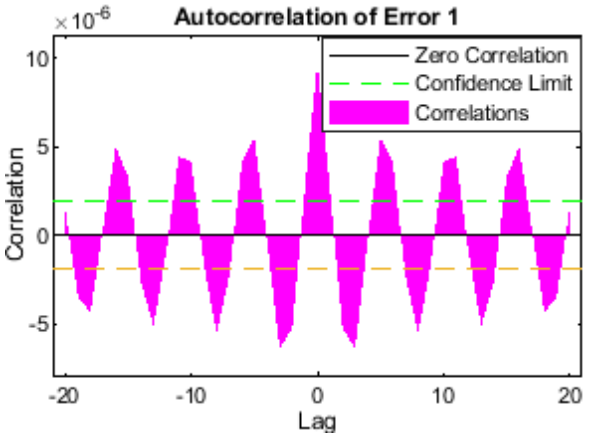

(f) Result of autocorrelation for scenario 2 with case 3

Figure 7. Comparison of mean square error (MSE) and auto-correlation for the various parameter value of case 1–3 based on malaria model with scenario 2.

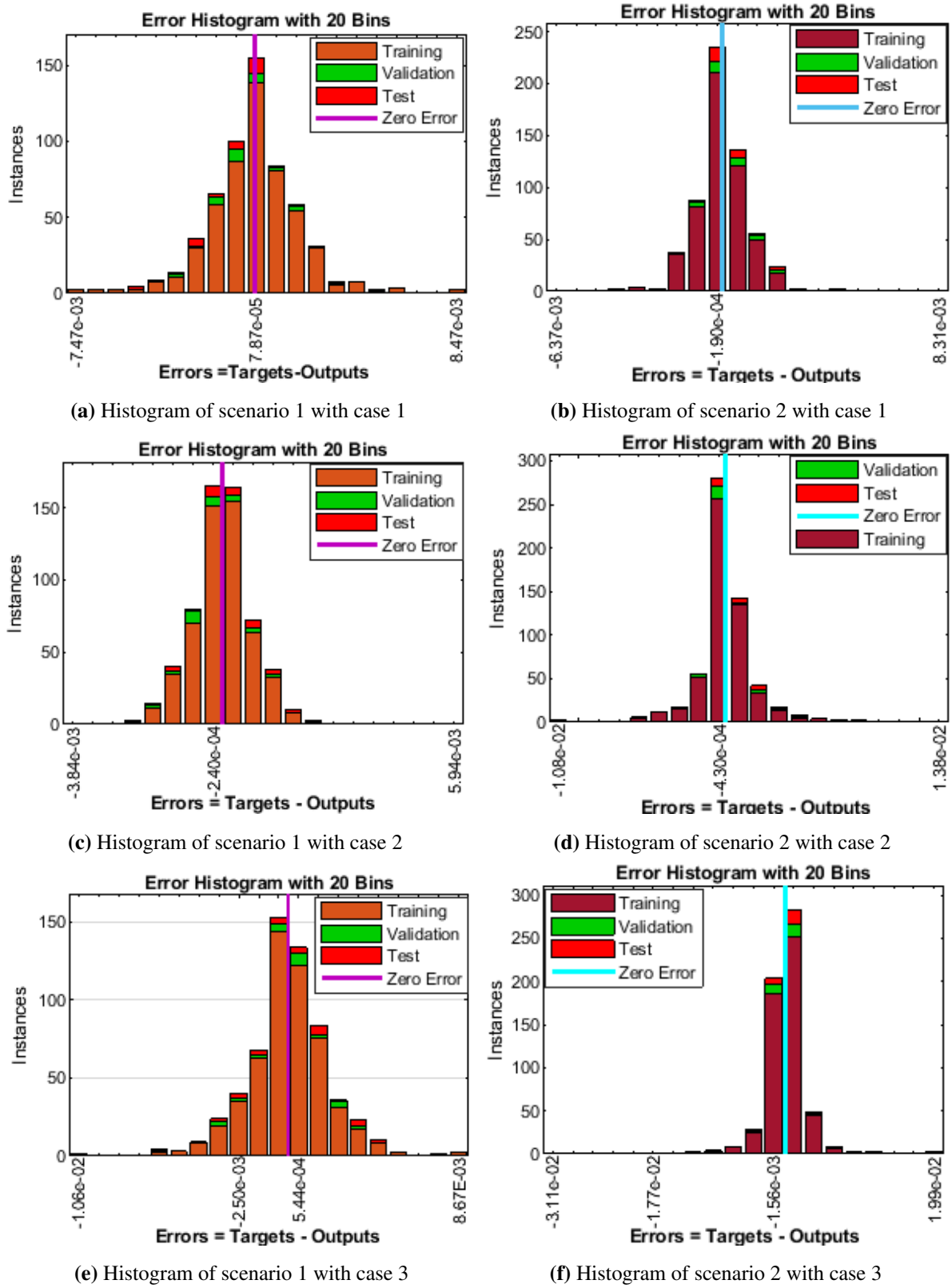

(a) Histogram of scenario 1 with case 1

(b) Histogram of scenario 2 with case 1

(c) Histogram of scenario 1 with case 2

(d) Histogram of scenario 2 with case 2

(e) Histogram of scenario 1 with case 3

(f) Histogram of scenario 2 with case 3

Figure 8. Comparison of error histogram for various parameter value of case 1–3 based on malaria model with scenario 1 and 2.

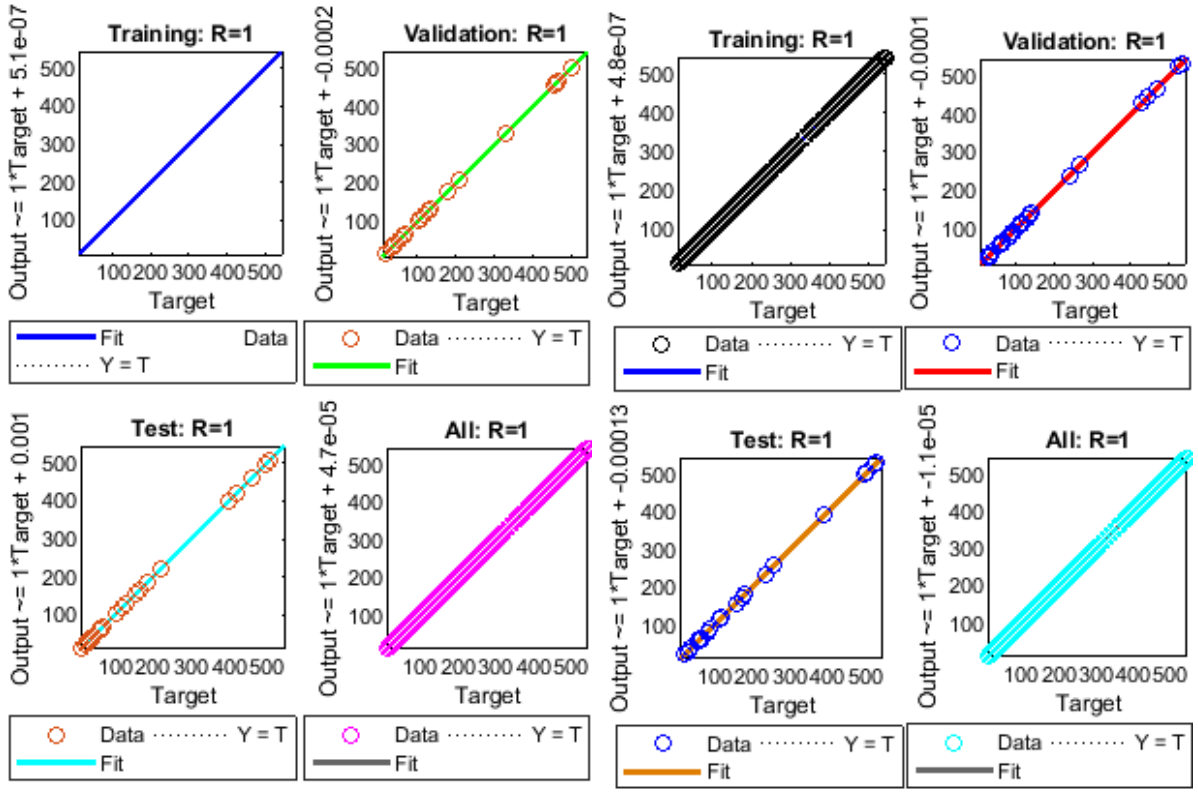

(a) Regression of case 1 with scenario 1

(b) Regression of case 1 with scenario 2

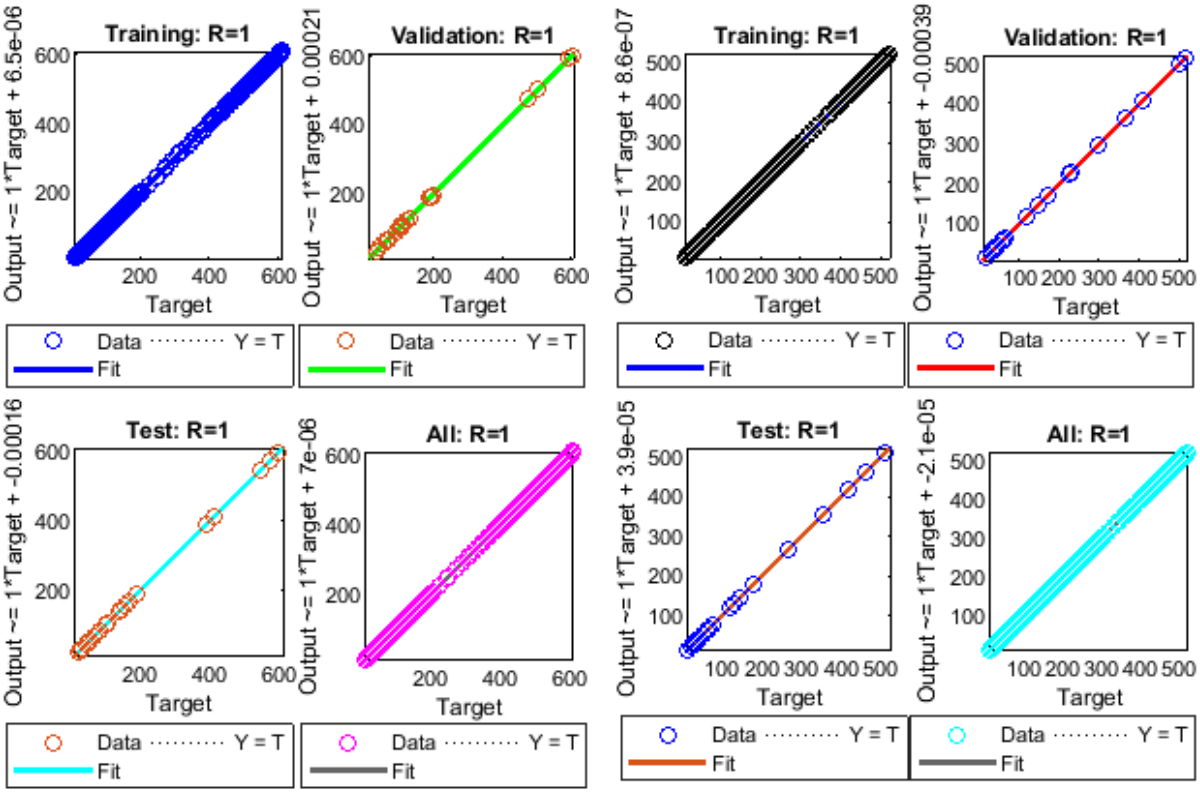

(c) Regression of case 2 with scenario 1

(d) Regression of case 2 with scenario 2

Figure 9. Comparison of regression for case 1-2 based on malaria model with scenario 1-2.

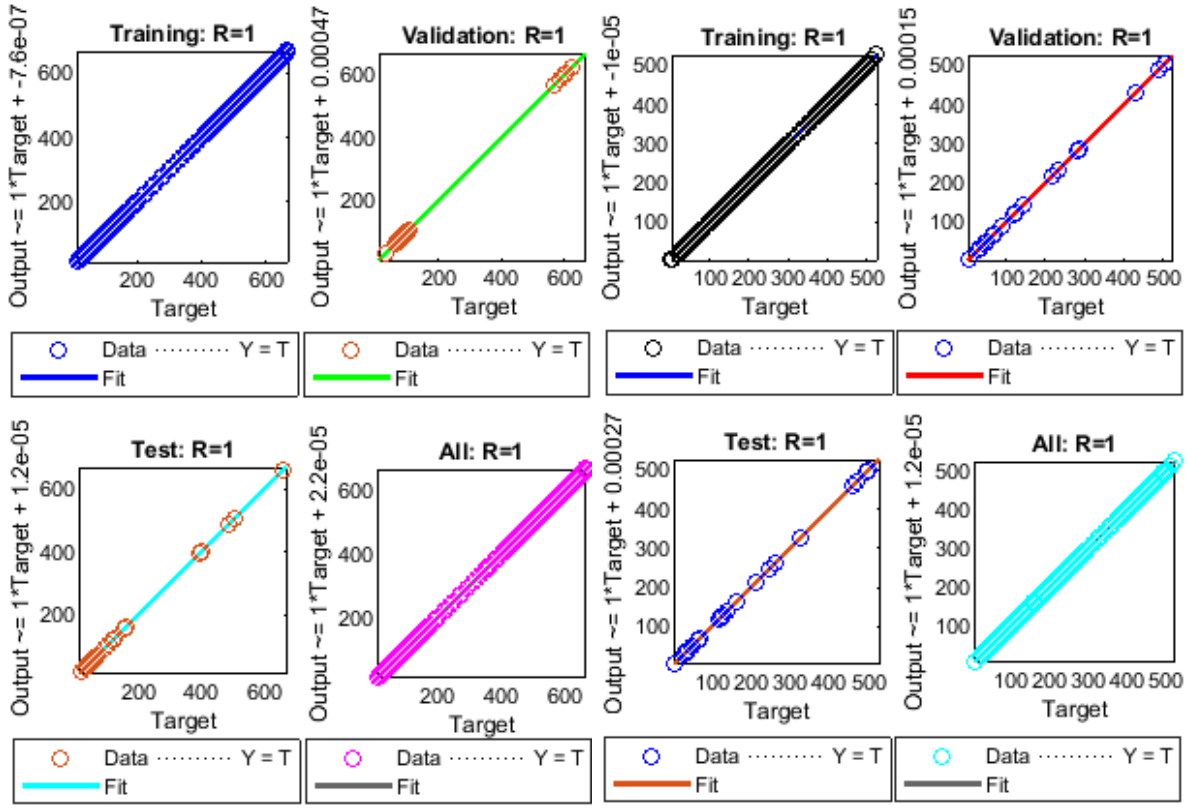

(a) Regression of case 3 with scenario 1 **(b)** Regression of case 3 with scenario 2

Figure 10. Comparison of regression for various parameter value of case 3 based on malaria model with scenario 1 and 2.

It is noted that Figure 6c of the malaria model describes better performance with scenario 2 as compared to other cases of both scenario because the mean square error (MES) of case 2 is the smallest best validation performance (BVP = 7.817×10^{-07} at epoch 1000). Figures 6a, 6c, 6e, 7a, 7c and 7e display the performance of all remaining cases with best validation performance 3.6665×10^{-06}, 5.5209×10^{-06}, 9.1707×10^{-07}, 3.5802×10^{-06}, 7.5891×10^{-06} along with 764, 554, 1000, 635 and 440 respectively. MSE has specific values for training, testing, and validating of both scenarios in every case of malaria model are shown in Table 2 respectively. Figures 6b, 6, d, 6f, 7b, 7d and 7f show the auto-correlation of both scenarios with three different cases. In the graph we define the correlation through the area. For each input point, the error dynamics are additionally estimated using an error histogram and the results of the graphically are presented in sub-Figure 8a-f of the malaria model.

The reference zero-line error bin has an error of around [7.8×10^{-05}, -2.4×10^{-04}, 5.4×10^{-04}, -1.9×10^{-04}, -4.3×10^{-04}, and -1.5×10^{-03}] for various cases, respectively. Specifies the value of the maximum result of the proposed method on the zero lines. In sub-Figures 9a-d and 10a-b describes the analysis of regression plots for validation, testing, and training of the malaria model. Regression value (R=1) indicates that during computation, there is a very close correlation between output and target values.

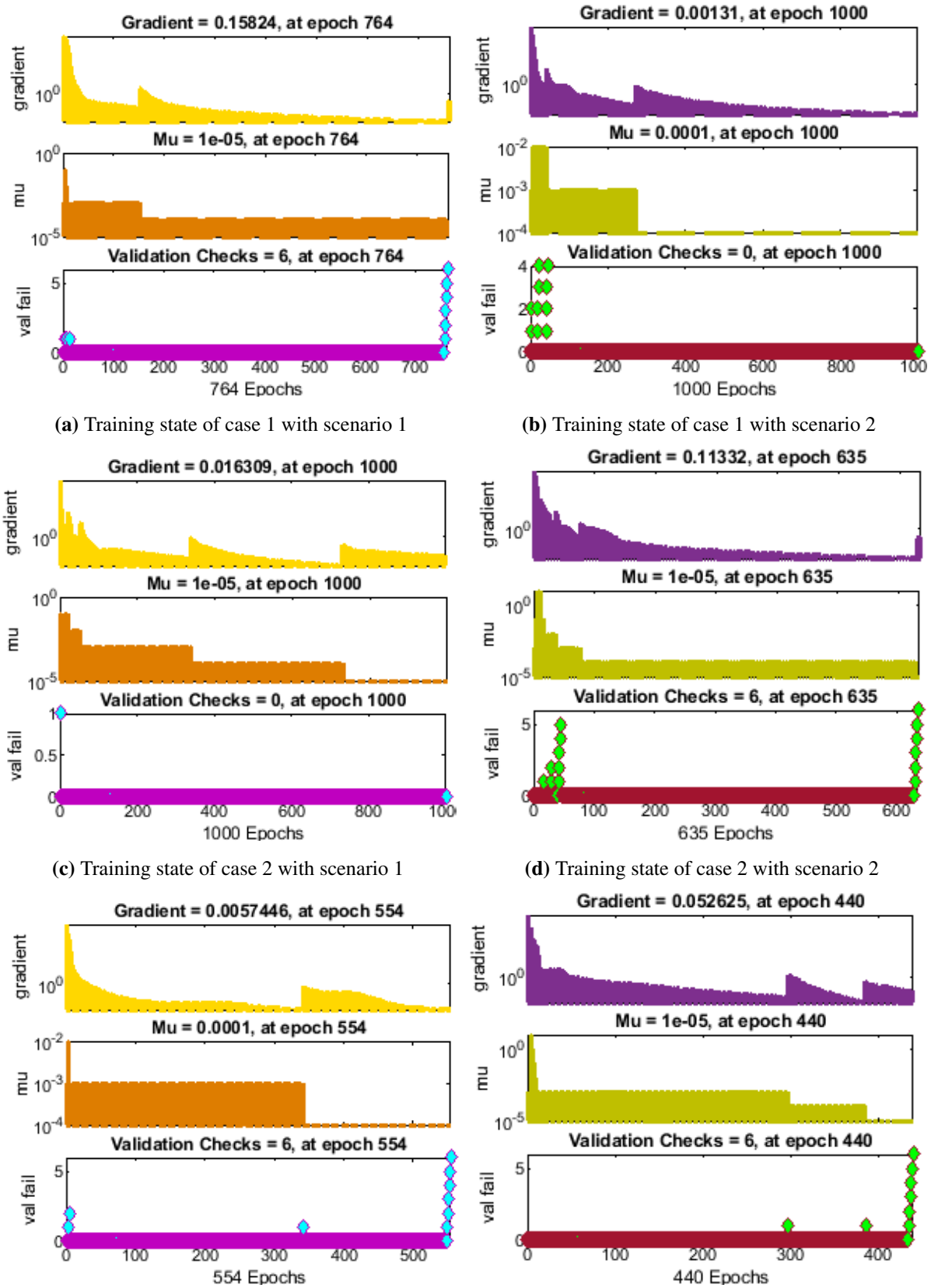

(a) Training state of case 1 with scenario 1

(b) Training state of case 1 with scenario 2

(c) Training state of case 2 with scenario 1

(d) Training state of case 2 with scenario 2

(e) Training state of case 3 with scenario 1

(f) Training state of case 3 with scenario 2

Figure 11. Analysis of training state for case 1–3 based on malaria model with scenario 1-2.

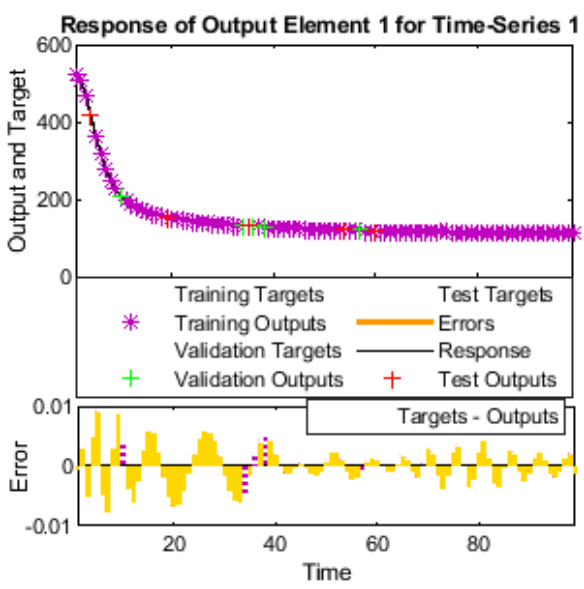

(a) Fitness plot of case 1 with scenario 1

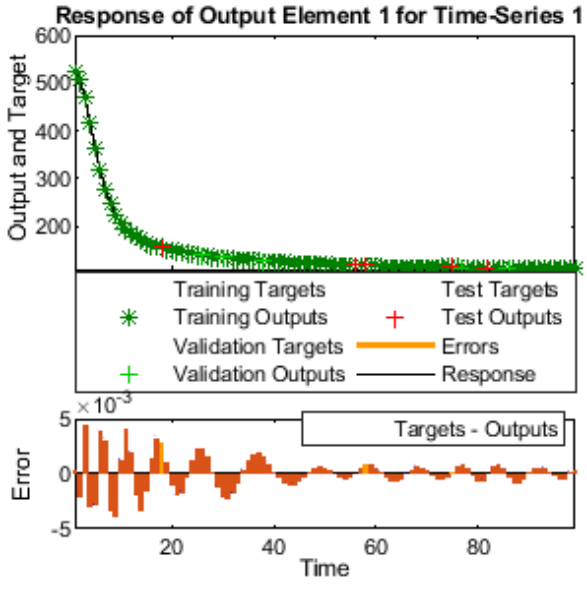

(b) Fitness plot of case 1 with scenario 2

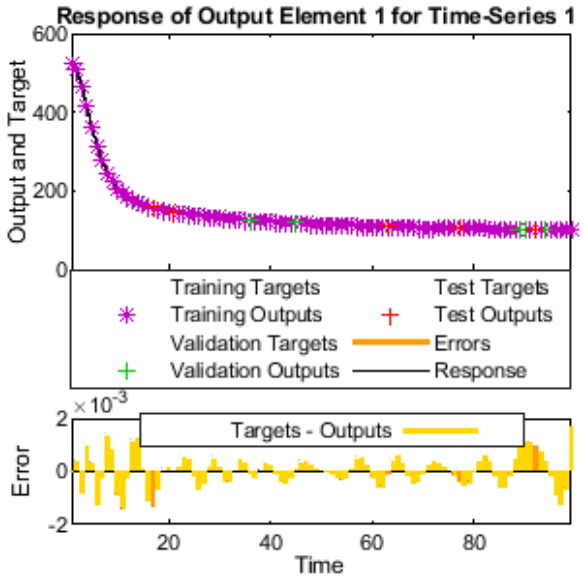

(c) Fitness plot of case 2 with scenario 1

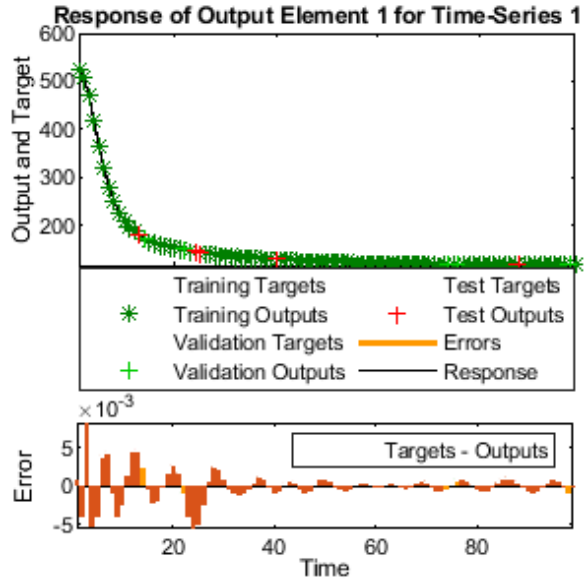

(d) Fitness plot of case 2 with scenario 2

Figure 12. Analysis of training state for case 1–3 based on malaria model with scenario 1-2.

Figure 11a-f display the training state of both scenarios with three different case. The training state show the better convergence rate. The value of both Mu and gradient corresponding to epoch show either the convergence is slow or fast. Furthermore, for all three cases of the malaria model through LMANNs, the convergence parameter achieved in terms of execution time, MSE, executed epochs, back-propagation, Mu step-size, and performance is tabulated in Tables 2 and the time of all cases describes the complexity of the suggested process. The back-propagation of step-size Mu and gradient values are about [10^{-05}, 10^{-05}, 10^{-05}, 10^{-04}, 10^{-05} and 10^{-05}] and [1.58×10^{-01}, 1.63×10^{-02}, 5.74×10^{-03}, 1.31×10^{-03}, 1.13×10^{-01} and 5.26×10^{-02}] as shown in sub Figure 11a–f for case 1–3 with

both scenario, respectively witch shows the convergence for all scenarios along all case of the proposed model through the designed solver is good.

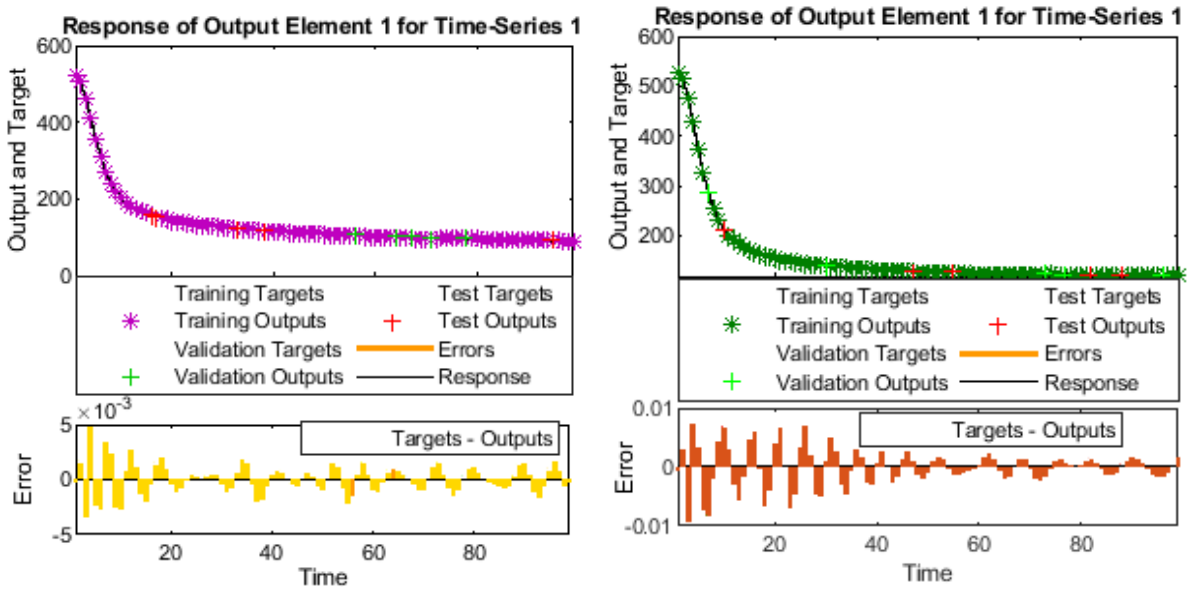

(a) Fitness plot of case 3 with scenario 1

(b) Fitness plot of case 3 with scenario 2

Figure 13. Analysis of training state for case 1–3 based on malaria model with scenario 1-2.

Table 2. An analysis of the malaria models constant parameters and their numerical values [44].

Sr.	Case	Time	Training	Testing	Validation	Performance	Gradient	Mu	Epochs
	1	7	4.1839 E-06	4.7212 E-06	3.6665 E-06	3.92 E-06	1.58 E-01	1.0 E-05	764
1	2	12	6.7394 E-07	1.2779E-06	7.8169 E-07	6.74 E-07	1.63 E-02	1.0 E-05	1000
	3	7	4.0440 E-06	5.5209 E-06	6.7520 E-06	3.97 E-06	5.74 E-03	1.0 E-05	554
	1	8	1.3049 E-06	1.0295 E-06	9.1707 E-07	1.30 E-06	1.31 E-03	1.0 E-04	1000
2	2	6	3.3948 E-06	1.0019 E-06	3.5802 E-06	3.15 E-06	1.13 E-01	1.0 E-05	635
	3	7	9.7834 E06	1.2531 E-05	7.5891 E-06	9.13 E-06	5.26 E-02	1.0 E-05	440

Table 3. Numerical value for all malaria model classes in case 1 with scenario 1.

Time	S1	I1	R1	R2	S2	I2
2	522.664700	111.683800	10.295100	20.847790	42.140950	49.145500
20	154.687700	397.825500	23.313140	59.600800	57.315190	35.957400
40	128.936900	468.748800	43.327700	119.339300	64.513980	31.715900
60	119.344200	504.681400	64.660130	183.060900	66.418080	30.581700
80	114.023100	527.573500	86.195060	247.273700	66.603650	30.279700
100	110.481700	544.144400	107.472800	310.543900	66.326200	30.199800

Table 4. Numerical value for all malaria model classes in case 2 with scenario 1.

Time	S1	I1	R1	R2	S2	I2
2	522.06370	112.44210	10.29530	20.05240	42.14060	49.14480
20	152.22690	404.61980	23.46260	50.09040	57.31130	35.95760
40	124.23480	487.09400	44.06840	93.73630	64.50090	31.71510
60	112.12350	537.86490	66.60800	135.13210	66.37660	30.58190
80	104.31010	577.37950	90.04990	171.93110	66.52300	30.27970
100	98.48940	611.03090	113.95860	204.00170	66.18720	30.19990

For every case of the malaria model, the results define the convergent performance and accuracy of the proposed system. The small Mu value can be observed to lead the better convergent outcomes. The analysis of fitness plots for the malaria model is shown in sub-Figures 12a-d and 13a-b, the error defined is the difference between target and output for testing, training, and validation at every scenario of input data-set point of malaria model.

The results obtained through LMANNs correspond to the reference (ref) of the Adams numerical solution in every case for all six groups of the malaria model, so absolute errors (AEs) are calculated to access the accuracy gauges. The absolute error (AEs) of all classes are shown in sub-Figure 14a–f and 15a–f for S_1, I_1, R_1, R_2, S_2 and I_2 respectively, for scenarios 1-2 tabular in Tables 9–14. The range of absolute error for Susceptible people class (S_1) is 10^{-03} to 10^{-04} of case 1 and 3 for scenario 1 and case 1 for scenario 2, 10^{-03} to 10^{-05} of case 2 for both scenario and 10^{-03} to 10^{-04}, 10^{-06} of case 3 for scenario 2 respectively. The range absolute error for infection people class (I_1) is 10^{-03} to 10^{-04} of case 1 2 and 3 for both scenario and 10^{-03} to 10^{-05} of case 2 for scenario 2 respectively. The range of absolute error for pseudo recovered people class (R_1), recovered people prone to re-infection class (R_2), mosquito susceptible class (S_2) and mosquito infection class (I_2) are 10^{-03} to 10^{-04}, 10^{-04} to 10^{-05} and 10^{-03} to 10^{-06} of case 1 for both scenario, 10^{-04}, 10^{-03} to 10^{-05}, 10^{-03} to 10^{-04}, 10^{-04} to 10^{-05} of case 2 for both scenario, 10^{-03} to 10^{-04}, 10^{-03} to 10^{-05} of case 3 for both scenarios respectively. The consistency of the suggested technique is shown by these ranges of absolute error for all groups of each case with both scenario, which is up to 10 decimal places.

Table 5. Numerical value for all malaria model classes in case 3 with scenario 1.

Time	S1	I1	R1	R2	S2	I2
2	522.66370	111.68510	10.29295	20.84474	42.14024	49.14545
20	154.68150	397.82150	23.30994	59.60180	57.31233	35.95972
40	128.94010	468.74800	43.32738	119.33990	64.51462	31.71600
60	119.34470	504.67770	64.66362	183.06130	66.41765	30.58183
80	114.02090	527.57560	86.19786	247.27580	66.60480	30.27979
100	110.48010	544.14320	107.47840	310.53990	66.32390	30.19985

Table 6. Numerical value for all malaria model classes in case 1 with scenario 2.

Time	S1	I1	R1	R2	S2	I2
2	522.66370	111.68510	10.29295	20.84474	42.14024	49.14545
20	154.68150	397.82150	23.30994	59.60180	57.31233	35.95972
40	128.94010	468.74800	43.32738	119.33990	64.51462	31.71600
60	119.34470	504.67770	64.66362	183.06130	66.41765	30.58183
80	114.02090	527.57560	86.19786	247.27580	66.60480	30.27979
100	110.48010	544.14320	107.47840	310.53990	66.32390	30.19985

Table 7. Numerical value for all malaria model classes in case 2 with scenario 2.

Time	S1	I1	R1	R2	S2	I2
2	523.02000	111.23160	9.81475	20.84186	42.14138	49.14421
20	156.17700	393.79430	17.26435	59.32878	57.41004	35.95924
40	131.77870	458.33170	26.79951	118.05050	64.84626	31.71193
60	123.57210	487.09770	33.96635	179.81170	67.07518	30.58100
80	119.45720	503.29470	38.94678	241.16040	67.62930	30.27778
100	116.85930	514.23930	42.34726	300.83440	67.73335	30.19689

Table 8. Numerical value for all malaria model classes in case 3 with scenario 2.

Time	S1	I1	R1	R2	S2	I2
2	526.02840	107.74570	6.08169	20.81147	42.17661	49.14320
20	158.80800	387.26660	3.38584	58.63798	57.62770	35.95841
40	134.76920	448.12890	4.07149	116.16140	65.31190	31.71772
60	126.54640	475.69770	4.36559	176.43680	67.72305	30.58002
80	122.10640	492.47110	4.53281	236.35900	68.39706	30.27578
100	119.07500	504.77440	4.65341	294.83760	68.57737	30.19504

Table 9. Absolute error (AEs) for all malaria model classes in case 1 with scenario 1.

Time	S1	I1	R1	R2	S2	I2
2	5.7100E-04	2.2000E-03	2.0800E-03	2.5000E-03	7.9900E-04	4.4700E-04
20	5.2500E-03	3.0100E-03	2.3100E-03	4.0400E-04	1.6400E-03	3.2800E-04
40	4.1400E-03	3.2400E-04	4.1000E-04	3.9200E-04	1.6800E-03	7.0600E-04
60	1.4200E-03	1.4700E-03	2.9400E-03	5.6900E-04	3.5600E-04	1.4800E-04
80	2.3300E-03	1.0200E-03	2.6400E-03	9.4300E-04	1.1100E-03	8.0900E-05
100	1.2800E-03	5.8400E-04	5.9900E-03	1.7300E-03	2.2500E-03	1.0100E-04

Table 10. Absolute error (AEs) for all malaria model classes in case 2 with scenario 1.

Time	S1	I1	R1	R2	S2	I2
2	1.5500E-05	8.9500E-04	3.5300E-04	1.9000E-04	4.4000E-04	2.5000E-04
20	4.9600E-05	1.6400E-03	1.8300E-04	1.7700E-04	1.6700E-04	9.5500E-05
40	2.9400E-04	6.8100E-04	1.1200E-04	2.2200E-04	1.1500E-04	9.9500E-05
60	2.7000E-04	4.4000E-04	3.2000E-04	1.4300E-03	9.3600E-05	1.2200E-04
80	4.5000E-04	4.1900E-04	6.9800E-04	6.8200E-04	4.1300E-04	2.4000E-04
100	1.7100E-03	5.7200E-04	8.5200E-04	1.2800E-03	1.2400E-04	8.6800E-05

Table 11. Absolute error (AEs) for all malaria model classes in case 3 with scenario 1.

Time	S1	I1	R1	R2	S2	I2
2	2.8400E-04	7.0800E-04	1.6200E-04	1.2600E-03	3.8700E-03	4.3000E-03
20	1.0000E-03	1.6500E-03	9.3500E-04	1.5500E-03	4.6100E-04	1.8100E-03
40	6.7600E-04	2.0300E-03	2.8600E-03	4.6500E-03	1.1500E-03	1.0300E-03
60	4.7400E-04	2.0600E-04	1.2100E-03	3.0000E-03	8.8100E-04	1.0500E-03
80	9.8800E-04	1.3000E-03	7.8100E-05	2.9500E-04	5.3000E-04	6.6500E-04
100	2.8000E-04	1.4600E-04	5.5700E-03	1.1500E-03	1.0800E-03	1.6100E-03

Table 12. Absolute error (AEs) for all malaria model classes in case 1 with scenario 2.

Time	S1	I1	R1	R2	S2	I2
2	3.7400E-04	8.5600E-04	8.4200E-05	5.7200E-04	8.8800E-05	3.9500E-04
20	1.0300E-03	1.0300E-03	8.8600E-04	5.9200E-04	1.2200E-03	2.0000E-03
40	9.3000E-04	1.1300E-03	7.3100E-04	1.0600E-03	1.0400E-03	8.1800E-04
60	8.9300E-04	2.2600E-03	5.5300E-04	9.6800E-04	7.0200E-05	6.5900E-05
80	1.5800E-04	1.0800E-03	1.6400E-04	1.1500E-03	4.5100E-05	6.3200E-06
100	3.1400E-04	1.7600E-03	4.4000E-04	2.3300E-03	5.0000E-05	9.2500E-05

Table 13. Absolute error (AEs) for all malaria model classes in case 2 with scenario 2.

Time	S1	I1	R1	R2	S2	I2
2	7.8600E-04	2.7700E-03	6.4500E-04	2.0200E-05	2.7700E-03	8.4500E-04
20	1.7400E-03	4.5800E-03	1.8900E-03	1.4200E-03	1.1000E-03	1.7000E-03
40	2.4800E-04	2.0800E-03	4.0000E-03	1.0300E-03	1.7100E-03	2.5800E-03
60	5.6100E-05	6.2800E-05	7.2700E-04	1.0600E-04	6.2100E-04	4.1800E-04
80	1.4400E-05	3.6900E-05	2.0200E-04	7.7400E-04	2.4200E-04	2.4700E-05
100	2.9100E-04	1.8400E-04	4.0600E-05	2.4100E-04	1.8700E-04	4.8900E-05

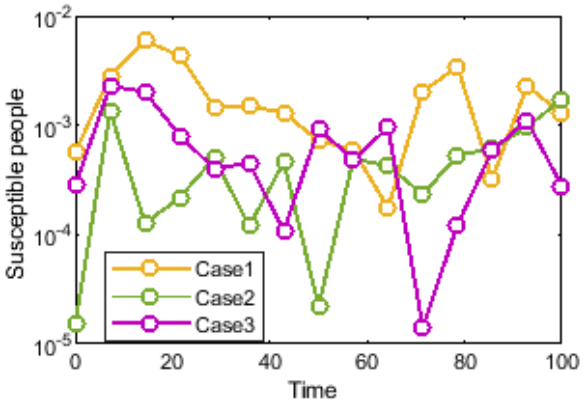

(a) Absolute error of S_1 for scenario 1

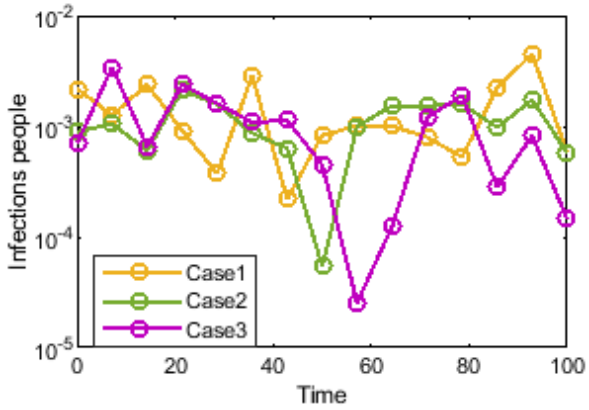

(b) Absolute error of I_1 for scenario 1

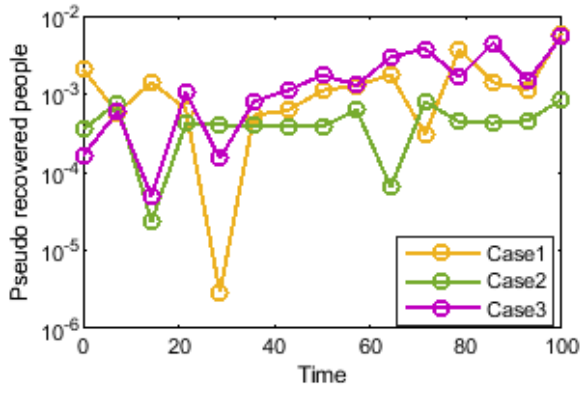

(c) Absolute error of R_1 for scenario 1

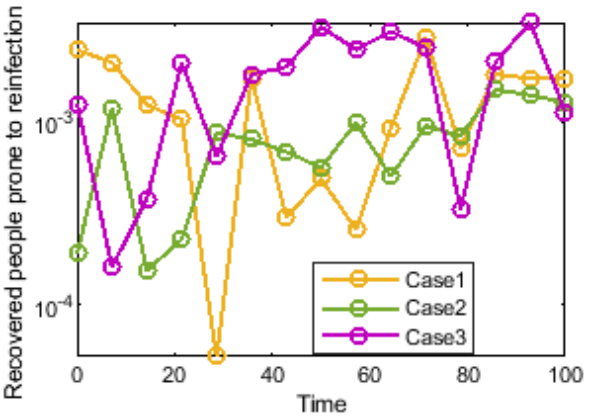

(d) Absolute error of R_2 for scenario 1

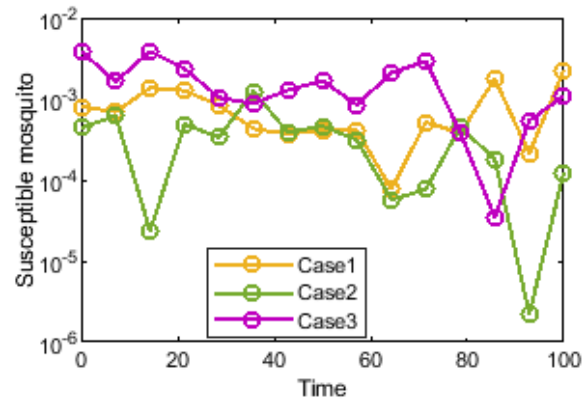

(e) Absolute error of S_2 for scenario 1

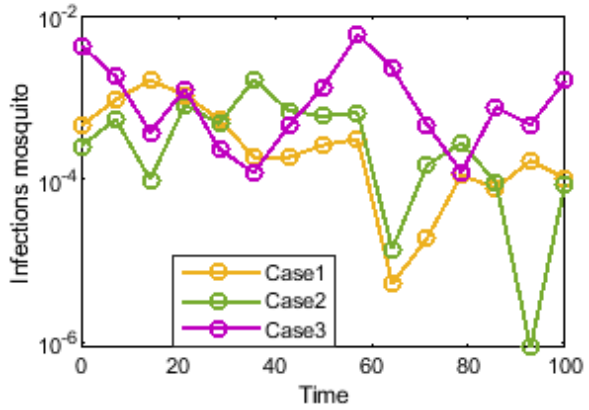

(f) Absolute error of I_2 for scenario 1

Figure 14. Comparison of absolute error for all classes of malaria model for case 1-3 with scenario 1.

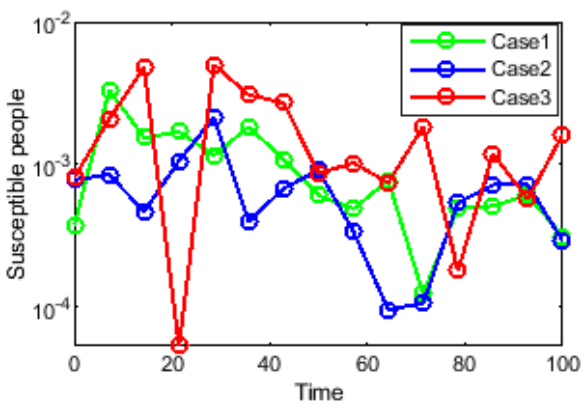

(a) Absolute error of S_1 for scenario 2

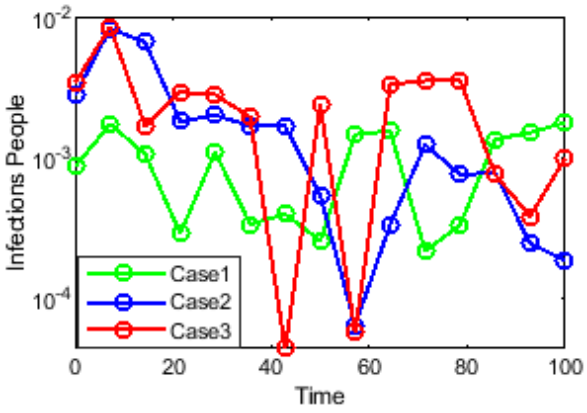

(b) Absolute error of I_1 for scenario 2

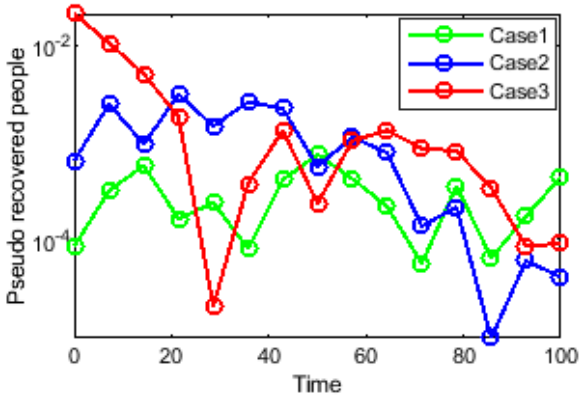

(c) Absolute error of R_1 for scenario 2

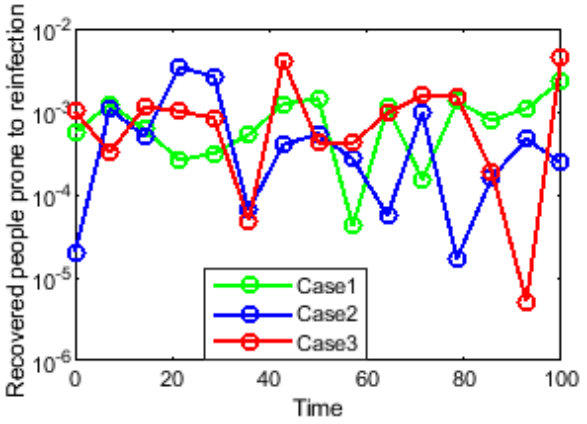

(d) Absolute error of R_2 for scenario 2

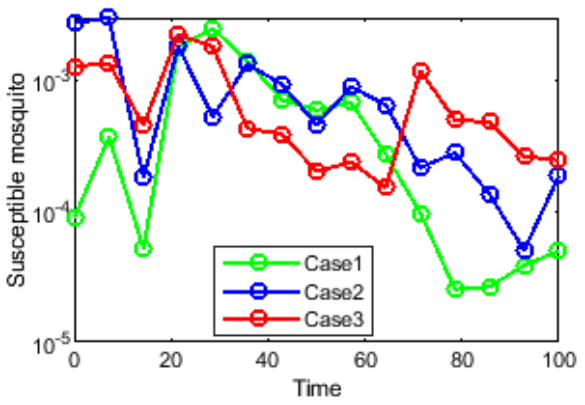

(e) Absolute error of S_2 for scenario 2

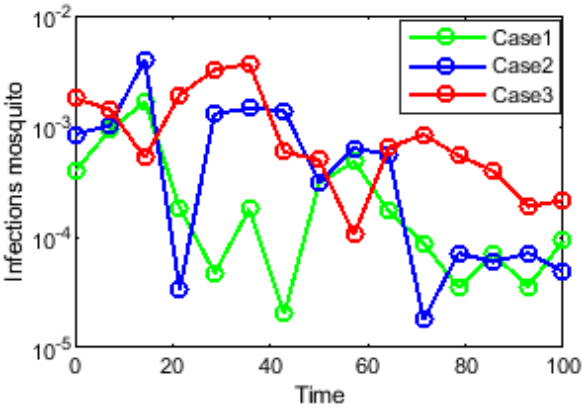

(f) Absolute error of I_2 for scenario 2

Figure 15. Comparison of absolute error for all classes of malaria model for case 1-3 with scenario 2.

Table 14. Absolute error (AEs) for all malaria model classes in case 3 with scenario 2.

Time	S1	I1	R1	R2	S2	I2
2	8.1100E-04	3.3800E-03	2.1400E-03	1.0000E-03	1.2900E-03	1.7900E-03
20	4.1000E-03	4.6500E-03	1.7700E-03	1.0400E-03	1.7900E-03	1.3200E-03
40	3.1100E-03	3.2400E-03	6.3500E-04	2.0400E-04	5.6900E-04	4.1300E-03
60	4.2500E-04	3.7200E-03	7.8700E-04	1.2000E-03	5.7000E-04	7.2900E-04
80	7.3100E-06	4.0800E-03	7.1000E-04	1.5400E-03	3.3600E-04	4.3900E-04
100	1.6200E-03	9.8100E-04	9.0500E-05	4.4000E-03	2.4600E-04	2.1500E-04

5. Conclusions

Through neural networks with Levenberg-Marquardt back-propagation, the integrated computing intelligent platform is presented to obtain the solution of the malaria mathematical model representing the spread of malaria that is constructed based on a real dataset. The input dataset for the malaria disease has been developed using the Adams numerical solver for various groups. The 5%, 5%, and 90% of reference data-sets are used as validation, testing, and training for LMANNs. The following key findings of the malaria model can be observed based on the above numerical analysis and investigation.

- ODEs representing the radioactive spread of the malaria disease are analyzed with the support of LMANN.
- Comparing the offered results with the numerical outcomes obtained by Adams method up-to 11 decimal point shows the consistency and accuracy of the suggested LMANNs.
- The feature of the suggested approach is further validated by numerically and graphically explanation based on error histogram, regression dynamics, mean square error and Convergence plots.
- The dynamics of malaria model are greatly influenced by the variation of parameters of interest.
- The efficiency of the computational process improves due to complexity mean square error (MSE), time series, regression, and histogram.

The designed solver LMANN for the analysis of structures representing the fluid flow systems [45–50] could be implemented in the future.

Acknowledgments

The authors extend their appreciation to the Deanship of Scientific Research at King Khalid University (KKU) for funding this research project Number (R.G.P.2/248/43).

Conflict of interest

The authors declare that there are no conflicts of interest.

References

1. World Health Organization. World malaria report 2015. World Health Organization, 2016. http://www.who.int/malaria/visual-refresh/en/

2. C. Chiyaka, J. M. Tchuenche, W. Garira, S. Dube, A mathematical analysis of the effects of control strategies on the transmission dynamics of malaria, *Appl. Math. Comput.,* **195** (2008), 641–662. https://doi.org/10.1016/j.amc.2007.05.016
3. K. Marsh, Malaria disaster in Africa, *Lancet,* **352** (1998), 924. https://doi.org/10.1016/S0140-6736(05)61510-3
4. World Health Organization, Diet, nutrition, and the prevention of chronic diseases: report of a joint WHO/FAO expert consultation, 916. World Health Organization, 2003. https://apps.who.int/iris/handle/10665/42665
5. S. W. Lindsay, W. J. Martens, Malaria in the African highlands: Past, present and future, *B. World Health Organ.*, **76** (1998), 33. https://www.ncbi.nlm.nih.gov/pmc/articles/PMC2305628/
6. K. O. Okosun, R. Ouifki, N. Marcus, Optimal control analysis of a malaria disease transmission model that includes treatment and vaccination with waning immunity, *Biosystems*, **106** (2011), 136–145. https://doi.org/10.1016/j.biosystems.2011.07.006
7. J. Popovici, L. Pierce-Friedrich, S. Kim, S. Bin, V. Run, D. Lek, er al., Recrudescence, reinfection, or relapse? A more rigorous framework to assess chloroquine efficacy for Plasmodium vivax malaria, *J. Infect. Dis.*, **219** (2019), 315–322. https://doi.org/10.1093/infdis/jiy484
8. Ric N. Price, L. von Seidlein, N. Valecha, F. Nosten, J. K. Baird, N. J. White, et al., Global extent of chloroquine-resistant Plasmodium vivax: A systematic review and meta-analysis, *Lancet Infect. Dis.*, **14** (2014), 982–991. https://doi.org/10.1016/S1473-3099(14)70855-2
9. P. Georgescu, H. Zhang, A Lyapunov functional for a SIRI model with nonlinear incidence of infection and relapse, *Appl. Math. Comput.*, **219** (2013), 8496–8507. https://doi.org/10.1016/j.amc.2013.02.044
10. M. Kotepui, F. R. Masangkay, K. U. Kotepui, G, De Jesus Milanez, Misidentification of Plasmodium ovale as Plasmodium vivax malaria by a microscopic method: A meta-analysis of confirmed P. ovale cases, *Sci. Rep.*, **10** (2020), 1–13. https://doi.org/10.1038/s41598-020-78691-7
11. B. Nadjm, R. H. Behrens, Malaria: An update for physicians, *Infect. Dis. Clin. North Am.*, **26** (2012), 243–259. https://doi.org/10.1016/j.idc.2012.03.010
12. R. Anguelov, Y. Dumont, J. Lubuma, Mathematical modeling of sterile insect technology for control of anopheles mosquito, *Comput. Math. Appl.*, **64** (2012), 374–389. https://doi.org/10.1016/j.camwa.2012.02.068
13. M. Ghosh, Mathematical modelling of malaria with treatment, *Adv. Appl. Math. Mech.*, **5** (2013), 857–871. https://doi.org/10.1017/S2070073300001272
14. S. Olaniyi, O. S. Obabiyi, Qualitative analysis of malaria dynamics with nonlinear incidence function, *Appl. Math. Sci.* **8** (2014), 3889–3904. http://dx.doi.org/10.12988/ams.2014.45326
15. A. L. Mojeeb, J. Li, Analysis of a vector-bias malaria transmission model with application to Mexico, Sudan and Democratic Republic of the Congo, *J. Theor. Biol.*, **464** (2019), 72–84. https://doi.org/10.1016/j.jtbi.2018.12.033
16. R. M. Anderson, R. M. May, Infectious diseases of humans: dynamics and control, *Oxford university press*, 1992. ISBN-13: 978-0198540403

17. S. Lal, G. P. S. Dhillon, C. S. Aggarwal, Epidemiology and control of malaria, *Indian J. Pediatr.,* **66** (1999), 547–554. https://doi.org/10.1007/BF02727167

18. R. Ross, The prevention of malaria, John Murray, 1911. https://doi.org/10.1007/978-0-85729-115-8-12

19. A. M. Niger, A. B. Gumel, Mathematical analysis of the role of repeated exposure on malaria transmission dynamics, *Differ. Equat. Dyn. Syst.*, **16** (2008), 251–287. https://doi.org/10.1007/s12591-008-0015-1

20. J. Li, Y. Zhao, S. Li, Fast and slow dynamics of malaria model with relapse, *Math. Biosci.,* **246** (2013), 94–104. https://doi.org/10.1016/j.mbs.2013.08.004

21. H. Huo, G. Qiu, Stability of a mathematical model of malaria transmission with relapse, *Abstr. Appl. Anal.*, **2014** (2014), Hindawi. https://doi.org/10.1155/2014/289349

22. A. Lahrouz, H. El Mahjour, A. Settati, A. Bernoussi, Dynamics and optimal control of a non-linear epidemic model with relapse and curem, *Physica A,* **496** (2018), 299–317. https://doi.org/10.1016/j.physa.2018.01.007

23. L. Liu, J. Wang, X. Liu, Global stability of an SEIR epidemic model with age-dependent latency and relapse, *Nonlinear Anal-Real.*, **24** (2015), 18–35. https://doi.org/10.1016/j.nonrwa.2015.01.001

24. A. L. Mojeeb, J. Li. Analysis of a vector-bias malaria transmission model with application to Mexico, Sudan and Democratic Republic of the Congo, *J. Theor. Biol.*, **464** (2019), 72–84. https://doi.org/10.1016/j.jtbi.2018.12.033

25. M. Ghosh, S. Olaniyi, O. S. Obabiyi, Mathematical analysis of reinfection and relapse in malaria dynamics, *Appl. Math. Comput.*, **373** (2020), 125044. https://doi.org/10.1016/j.amc.2020.125044

26. H. Zhang, J. Guo, H. Li, Y. Guan, Machine learning for artemisinin resistance in malaria treatment across in vivo-in vitro platforms, *Iscience*, **25** (2022), 103910. https://doi.org/10.1016/j.isci.2022.103910

27. R. Islam, Nahiduzzaman, O. F. Goni, A. Sayeed, S. Anower, M. Ahsan, et al., Explainable transformer-based deep learning model for the detection of Malaria Parasites from blood cell images, *Sensors*, **22** (2022), 4358. https://doi.org/10.3390/s22124358

28. M. A. Omoloye, A. E. Udokang, A. O. Sanusi, O. K. S. Emiola, Analytical solution of dynamical transmission of Malaria disease model using differential transform method, *Int. J. Novel Res. Phys. Chem. Math.*, **9** (2022), 1–13. https://www.noveltyjournals.com/upload/paper/Analytical%20Solution-27042022-7.pdf

29. N. H. Sweilam, Z. N. Mohammed, Numerical treatments for a multi-time delay complex order mathematical model of HIV/AIDS and malaria, *Alex. Eng. J.*, **61** (2022), 10263–10276. https://doi.org/10.1016/j.aej.2022.03.058

30. I. Khan, M. A. Z. Raja, M. Shoaib, P. Kumam, H. Alrabaiah, Z. Shah, Design of neural network with Levenberg-Marquardt and Bayesian regularization backpropagation for solving pantograph delay differential equations, *IEEE Access*, **8** (2020), 137918–137933. https://doi.org/10.1109/ACCESS.2020.3011820

31. A. H. Bukhari, M. Sulaiman, M. A. Z. Raja, S. Islam, M. Shoaib, P. Kumam, Design of a hybrid NAR-RBFs neural network for nonlinear dusty plasma system, *Alex. Eng. J.*, **59** (2020), 3325–3345. https://doi.org/10.1016/j.aej.2020.04.051
32. I. Ahmad, H. Ilyas, A. Urooj, M. S. Aslam, M. Shoaib, M. A. Z. Raja, Novel applications of intelligent computing paradigms for the analysis of nonlinear reactive transport model of the fluid in soft tissues and microvessels, *Neural Comput. Appl.*, **31** (2019), 9041–9059. https://doi.org/10.1007/s00521-019-04203-y
33. Z. Shah, M. A. Z. Raja, Y. Chu, W. A. Khan, M. Waqas, M. Shoaih, et al., Design of neural network based intelligent computing for neumerical treatment of unsteady 3D flow of Eyring-Powell magneto-nanofluidic model, *J. Mater. Res. Technol.*, **9** (2020), 14372–14387. https://doi.org/10.1016/j.jmrt.2020.09.098
34. H. Ilyas, I. Ahmad, M. A. Z. Raja, M. Shoaib, A novel design of Gaussian WaveNets for rotational hybrid nanofluidic flow over a stretching sheet involving thermal radiation, *Int. Commun. Heat Mass Transfer*, **123** (2021), 105196. https://doi.org/10.1016/j.icheatmasstransfer.2021.105196
35. H. Ilyas, I. Ahmad, M. A. Z. Raja, M. B. Tahir, M. Shoaib, Intelligent networks for crosswise stream nanofluidic model with Cu-H_2O over porous stretching medium, *Int. J. Hydrogen Energ.*, **46** (2021), 15322–15336. https://doi.org/10.1016/j.ijhydene.2021.02.108
36. H. Ilyas, I. Ahmad, M. A. Z. Raja, M. B. Tahir, M. Shoaib, Intelligent computing for the dynamics of fluidic system of electrically conducting Ag/Cu nanoparticles with mixed convection for hydrogen possessions, *Int. J. Hydrogen Energ.*, **46** (2021), 4947–4980. https://doi.org/10.1016/j.ijhydene.2020.11.097
37. T. N. Cheema, M. A. Z. Raja, I. Ahmad, S. Naz, H. Ilyas, M. Shoaib, Intelligent computing with Levenberg–Marquardt artificial neural networks for nonlinear system of COVID-19 epidemic model for future generation disease control, *Europ. Phys. J. Plus*, **135** (2020), 1–35. https://doi.org/10.1140/epjp/s13360-020-00910-x
38. M. Shoaib, M. A. Z. Raja, M. T. Sabir, A. H. Bukhari, H. Alrabaiah, Z. Shah, A stochastic numerical analysis based on hybrid NAR-RBFs networks nonlinear SITR model for novel COVID-19 dynamics, *Comput. Meth. Prog. Bio.*, **202** (2021), 105973. https://doi.org/10.1016/j.cmpb.2021.105973
39. Z. Sabir, M. A. Z. Raja, J. L. G. Guirao, M. Shoaib, A novel design of fractional Meyer wavelet neural networks with application to the nonlinear singular fractional Lane-Emden systems, *Alex. Eng. J.*, **60** (2021), 2641–2659. https://doi.org/10.1016/j.aej.2021.01.004
40. I. Khan, M. A. Z. Raja, M. Shoaib, P. Kumam, H. Alrabaiah, Z. Shah, SCL 802 Fixed Point Laboratory, Center of Excellence in Theoretical and Computational Science (TaCS-CoE), King Mongkut's University of Technology, Thonburi (KMUTT), Bangkok, Thailand Design of neural network with Levenberg-Marquardt and Bayesian regularization backpropagation for solving pantograph delay differential equations, *IEEE Access*, **8** (2020), 137918–137933. https://doi.org/10.1109/ACCESS.2020.3011820
41. Z. Sabir, D. Baleanu, M. Shoaib, M. A. Z. Raja, Design of stochastic numerical solver for the solution of singular three-point second-order boundary value problems, *Neural Comput. Appl.*, **33** (2021), 2427–2443. https://doi.org/10.1007/s00521-020-05143-8

42. Z. Sabir, M. Umar, J. L. G. Guirao, M. S. Muhammad A. Z. Raja, Integrated intelligent computing paradigm for nonlinear multi-singular third-order Emden Fowler equation, *Neural Comput. Appl.*, **33** (2021), 3417–3436. https://doi.org/10.1007/s00521-020-05187-w
43. Z. Sabir, M. A. Z. Raja, M. Shoaib, J. F. Gómez Aguilar, FMNEICS: Fractional Meyer neuro-evolution-based intelligent computing solver for doubly singular multi-fractional order Lane Emden system, *Comput. Appl. Math.*, **39** (2020), 1–18. https://doi.org/10.1007/s40314-020-01350-0
44. D. I. Wallace, B. S. Southworth, X. Shi, J. W. Chipman, A. K. Githeko, A comparison of five malaria transmission models: Benchmark tests and implications for disease control, *Malaria J.*, **13** (2014), 1–16. https://doi.org/10.1186/1475-2875-13-268
45. I. Ahmad, T. N. Cheema, M. A. Z. Raja, S. E. Awan, N. B. Alias, S. Iqbal, et al., A novel application of Lobatto IIIA solver for numerical treatment of mixed convection nanofluidic model, *Sci. Rep.* **11** (2021), 1–16. https://doi.org/10.1038/s41598-021-83990-8
46. M. Shoaib, M. A. Z. Raja, M. T. Sabir, S. Islam, Z. Shah, P. Kumam, et al., Numerical investigation for rotating flow of MHD hybrid nanofluid with thermal radiation over a stretching sheet, *Sci. Rep.*, **10** (2020), 1–15. https://doi.org/10.1038/s41598-020-75254-8
47. O. Chun1, M. A. Z. Raja, S. Naz, I. Ahmad, R. Akhtar, Y. Ali, et al., Dynamics of inclined magnetic field effects on micropolar Casson fluid with Lobatto IIIA numerical solver, *AIP Adv.*, **10**, (2020), 065023. https://doi.org/10.1063/5.0004386
48. C. Ouyang1, R. Akhtar, M. A. Z. Raja, M. T. Sabir, M. Awais, M. Shoaib, Numerical treatment with Lobatto IIIA technique for radiative flow of MHD hybrid nanofluid (Al2O3Cu/H2O) over a convectively heated stretchable rotating disk with velocity slip effects, *AIP Adv.*, **10** (2020), 055122. https://doi.org/10.1063/1.5143937
49. M. Shoaib, M. A. Z. Raja, M, T, Sabir, M. Awais, S. Islam, Z. Shah, et al., Numerical analysis of 3-D MHD hybrid nanofluid over a rotational disk in presence of thermal radiation with Joule heating and viscous dissipation effects using Lobatto IIIA technique, *Alex. Eng. J.*, **60** (2021), 3605–3619. https://doi.org/10.1016/j.aej.2021.02.015
50. M. Awais, M. A. Z. Raja, S. E. Awan, M. Shoaib, H. M. Ali, Heat and mass transfer phenomenon for the dynamics of Casson fluid through porous medium over shrinking wall subject to Lorentz force and heat source/sink, *Alex. Eng. J.*, **60** (2021), 1355–1363. https://doi.org/10.1016/j.aej.2020.10.056

AIMS Press